© 2019. Published by The Company of Biologists Ltd | Journal of Cell Science (2019) 132, jcs233379. doi:10.1242/jcs.233379

RESEARCH ARTICLE

First meiotic anaphase requires Cep55-dependent inhibitory cyclin-dependent kinase 1 phosphorylation

Chenxi Zhou[1], Janelle L. Hancock[2], Kum Kum Khanna[2] and Hayden A. Homer[1,*]

ABSTRACT

During mitosis, anaphase is triggered by anaphase-promoting complex (APC)-mediated destruction of securin and cyclin B1, which leads to inactivation of cyclin-dependent kinase 1 (Cdk1). By regulating APC activity, the mitotic spindle assembly checkpoint (SAC) therefore has robust control over anaphase timing to prevent chromosome mis-segregation. Mammalian oocytes are prone to aneuploidy, the reasons for which remain obscure. In mitosis, Cep55 is required post-anaphase for the final steps of cytokinesis. We found that Cep55-depleted mouse oocytes progress normally through early meiosis I, but that anaphase I fails as a result of persistent Cdk1 activity. Unexpectedly, Cdk1 inactivation was compromised following Cep55 depletion, despite on-time SAC silencing and intact APC-mediated proteolysis. We found that impaired Cdk1 inactivation was caused by inadequate inhibitory Cdk1 phosphorylation consequent upon failure to suppress Cdc25 phosphatase, identifying a proteolysis-independent step necessary for anaphase I. Thus, the SAC in oocytes does not exert exclusive control over anaphase I initiation, providing new insight into vulnerability to error.

KEY WORDS: Anaphase I, Oocytes, Anaphase-promoting complex, Meiosis, Cep55, Cdk1

INTRODUCTION

To prevent aneuploidy, the timing of anaphase must be finely tuned; such fine-tuning is the responsibility of the spindle assembly checkpoint (SAC) (Foley and Kapoor, 2013). In both mitosis and meiosis, anaphase occurs when the chromosomal glue, cohesin, is cleaved by the cysteine protease, separase (Hauf et al., 2001; Kudo et al., 2006; Terret et al., 2003). Activation of separase occurs following release from its inhibitory chaperone, securin (Waizenegger et al., 2002), brought about through securin proteolysis orchestrated by the anaphase-promoting complex (APC) acting in concert with its cell-division cycle protein 20 (Cdc20) coactivator (Homer, 2013; Pesin and Orr-Weaver, 2008; Herbert et al., 2003). As separase is also inhibited by cyclin-dependent kinase 1 (Cdk1) (Stemmann et al., 2001), anaphase also requires APC-Cdc20-mediated destruction of the Cdk1 activator, cyclin B1 (Pesin and Orr-Weaver, 2008; Wolf et al., 2006). In addition to cyclin B1 availability, Cdk1 activity is controlled by inhibitory Wee1/Myt1 kinase (Wee1B in oocytes)-mediated phosphorylation of Cdk1 residues Thr14 and Tyr15, which are removed by Cdc25 phosphatases (Cdc25B in oocytes) (Han et al., 2005; Malumbres, 2014; Adhikari and Liu, 2014; Lincoln et al., 2002). Inhibitory Cdk1 phosphorylation reinforces mitotic exit in cellular extracts, but this involves altered proteolysis (D'Angiolella et al., 2007; Forester et al., 2007). APC-Cdc20-mediated proteolysis is therefore the principal anaphase driver during mitosis (Meadows and Millar, 2015; Sullivan and Morgan, 2007). Thus, by controlling the timing of APC-Cdc20 activation, the mitotic SAC has stringent control over proteolysis and, by extension, anaphase timing, to prevent aneuploidy.

Meiotic maturation in mouse oocytes involves two consecutive M phases, meiosis I (MI) and meiosis II (MII), without intervening nuclear reformation, culminating in MII arrest (Greaney et al., 2018). As in mitosis, anaphase I and exit from MI in mouse oocytes require APC-Cdc20-mediated proteolysis of securin and cyclin B1 (Greaney et al., 2018; Herbert et al., 2003; Jones and Lane, 2013). Although an SAC exists in oocytes (Hached et al., 2011; Homer et al., 2005a,b; Wassmann et al., 2003), MI in oocytes is nevertheless prone to error, especially with ageing (Greaney et al., 2018; Jones and Lane, 2013). One model for explaining this paradox is that the oocyte SAC lacks stringency (Greaney et al., 2018; Gui and Homer, 2012; Kolano et al., 2012; Lane et al., 2012; Sebestova et al., 2012), but why this should be is not clear.

During exit from mitosis, the final steps of cytokinesis (abscission) occur after nuclear envelope reformation and require Cep55 (Fabbro et al., 2005; Gershony et al., 2014; Zhao et al., 2006). Cep55 is a centrosome- and midbody-associated coiled-coil protein (Fabbro et al., 2005) that orchestrates the final stages of membrane abscission by directing the midbody recruitment of key proteins required for cytokinesis completion, such as tumour-susceptibility gene 101 (TSG101) and ALG2-interacting protein X (ALIX) (Martinez-Garay et al., 2006; Morita et al., 2007; van der Horst et al., 2009; Zhao et al., 2006). Consequently, when Cep55 is depleted in somatic cells, mitosis arrests at a late post-anaphase stage (Fabbro et al., 2005; van der Horst et al., 2009; Zhao et al., 2006).

Here, we set out to investigate Cep55 function during MI in mouse oocytes, given that nuclear envelopes do not reform during exit from MI. We found that anaphase I and subsequent MI exit events failed following Cep55 depletion, despite normal SAC inactivation and intact APC-Cdc20-mediated proteolysis. This was the result of sustained Cdk1 activity secondary to reduced inhibitory Cdk1 phosphorylation, identifying a crucial proteolysis-independent requirement for anaphase I. Thus, anaphase I requires separate proteolytic and non-proteolytic inputs, contrasting with the exclusively proteolysis-driven mitotic anaphase pathway. Because the SAC can robustly regulate the timing of anaphase onset only if anaphase is completely controlled by APC-Cdc20-mediated proteolysis, this puts chromosome segregation at risk in oocytes.

[1]The Christopher Chen Oocyte Biology Research Laboratory, UQ Centre for Clinical Research, The University of Queensland, Herston 4029, QLD, Australia. [2]Signal Transduction Laboratory, QIMR Berghofer Medical Research Institute, Herston, QLD, Australia.

*Author for correspondence (h.homer@uq.edu.au)

H.A.H., 0000-0002-3104-0449

Received 18 April 2019; Accepted 9 August 2019

Journal of Cell Science (2019) 132, jcs233379. doi:10.1242/jcs.233379

RESULTS

Cep55 depletion inhibits anaphase I

MI begins with breakdown of the oocyte nucleus (termed germinal vesicle breakdown, GVBD) and concludes with the first polar body extrusion (PBE). Western blotting showed that Cep55 levels were very low in early MI and became prominent by late MI (Fig. 1A). To investigate Cep55 function, we depleted Cep55 by microinjecting siRNAs previously shown to target murine *Cep55* effectively in somatic cells (Kalimutho et al., 2018). Cep55-targeting siRNAs depleted ∼80% of endogenous protein (Fig. 1B,C) and resulted in complete loss of Cep55 signals in immunostained oocytes (Fig. S1).

To investigate the impact of Cep55 knockdown on MI progression, we undertook timelapse imaging. Similarly high rates (∼80%) of GVBD were observed in Cep55- and mock-depleted oocytes (Fig. 1D) 2 h after washing from the GVBD inhibitor, 3-isobutyl-1-methylxanthine (IBMX). Notably, however, GVBD was markedly accelerated within the first 30 min post-release from IBMX (Fig. 1D). Importantly, therefore, we performed all subsequent comparisons of MI progression with strict reference to the time of GVBD. Exit from MI (PBE) occurred by 9-10 h post-GVBD in ∼80% of controls (Fig. 1E). Strikingly, however, only ∼20% of Cep55-depleted oocytes underwent PBE by the same time post-GVBD (Fig. 1E). This was specific to Cep55 depletion because co-expression of exogenous Cep55 from microinjected siRNA-resistant Cep55 cRNA completely restored PBE rates to ∼80% (Fig. 1F). Thus, Cep55 knockdown accelerated entry into MI but markedly inhibited MI exit.

Given the requirement of Cep55 for mitotic abscission (Fabbro et al., 2005; Zhao et al., 2006), we presumed that PBE inhibition following Cep55 knockdown was the result of a late post-anaphase I defect. To investigate this, we undertook timelapse imaging of fluorescently labelled spindles and chromosomes in live oocytes (Wei et al., 2018). Bipolar spindles assembled normally by 5-6 h post-GVBD and chromosome alignment at the spindle equator in Cep55-depleted oocytes was similar to that in mock-depleted controls (Fig. 1G; Fig. S1, Movies 1 and 2). Mock-depleted oocytes then progressed to anaphase I and PBE at around 7-9 h post-GVBD (Fig. 1E,G). Surprisingly, however, in Cep55-depleted oocytes, chromosome separation did not occur in ∼80% of oocytes, even after 19 h post-GVBD, well beyond the time that controls underwent anaphase I (Fig. 1E,G; Movies 1 and 2). Using chromosome spreads, we confirmed that homologous chromosome pairs had indeed remained intact in MI-arrested Cep55-depleted oocytes (Fig. 1H). Thus, Cep55 knockdown induced metaphase I arrest in oocytes, contrasting with the post-anaphase abscission defect in mitosis (Zhao et al., 2006).

The SAC is inactivated following Cep55 knockdown

We reasoned that anaphase I failure could be caused by inhibition of APC-Cdc20, as proteolysis of securin and cyclin B1 are understood to mediate chromosome segregation (Herbert et al., 2003; Homer, 2013; Meadows and Millar, 2015; Pesin and Orr-Weaver, 2008). Because APC-Cdc20 activity is inhibited by the SAC until chromosomes attach to spindle microtubules via kinetochores (Foley and Kapoor, 2013), we first asked whether the SAC remained chronically active following Cep55 depletion. An active SAC is signified by enrichment of the SAC protein, Mad2, at kinetochores (Gui and Homer, 2012; Waters et al., 1998; Lane et al., 2012). In Cep55-depleted oocytes, as in controls, unattached kinetochores during early MI (1-2 h post-GVBD when kinetochores are mostly unattached) recruited high levels of Mad2 (Fig. 2A). By 6-7 h post-GVBD in controls, after the spindle had bipolarised and chromosomes were placed under tension at the spindle equator (Fig. 1G; Fig. S1), Mad2 levels were largely undetectable, which is indicative of high kinetochore-microtubule occupancy and SAC silencing (Fig. 2A). Significantly, in Cep55-depleted oocytes, kinetochore Mad2 levels also dissipated over the same period, indicating that the SAC was being silenced normally (Fig. 2A). This was consistent with our earlier timelapse data which clearly showed that normal bipolar spindles assembled after Cep55 depletion and that chromosomes aligned at the spindle equator (Fig. 1G; Fig. S1), thereby satisfying conditions for silencing the SAC.

To investigate whether residual SAC activity might still be present despite normal Mad2 loss from kinetochores and chromosome alignment, we treated metaphase I-arrested Cep55 knockdown oocytes using a specific inhibitor (reversine) of Mps1, which is required for the SAC in oocytes (Hached et al., 2011). We found that reversine could not induce anaphase I or MI exit (Fig. 2B,C). Thus, anaphase I failure following Cep55 knockdown was not the result of persistent SAC activation.

APC-Cdc20-mediated proteolysis is unperturbed despite metaphase I arrest

Because SAC silencing should allow APC-Cdc20 to become active (Pesin and Orr-Weaver, 2008; Foley and Kapoor, 2013), the failure to induce anaphase I despite forced SAC inactivation (Fig. 2B,C) was surprising, leading us to ask whether APC-Cdc20 activity might be impacted in an SAC-independent manner by Cep55 depletion. To investigate this, we used timelapse fluorescence imaging of securin-GFP, whose destruction provides a readout of APC-Cdc20 activity (Homer et al., 2005b; Lane and Jones, 2014), to determine whether APC-Cdc20 was becoming active. Notably, however, a decline in securin-GFP fluorescence, reflecting onset of APC-Cdc20-mediated proteolysis, clearly occurred in Cep55-depleted oocytes and began at the same time (about 5-6 h post-GVBD) as in controls (Fig. 3A,B), consistent with above data showing on-time inactivation of the SAC. Furthermore, there was no difference in either extent or rate of proteolysis between the two groups (Fig. 3C,D). In keeping with our findings using exogenous securin-GFP, we also found that the majority of endogenous securin underwent destruction by 8 h post-GVBD in both Cep55-depleted and control oocytes (Fig. 3E). We confirmed that proteolysis was APC-mediated by using an APC-specific inhibitor, APCIN (Wei et al., 2018), which induced protein stabilisation in both mock- and Cep55-depleted oocytes (Fig. 3F).

It was unexpected that SAC inactivation and proteolysis remained completely intact despite metaphase I arrest. We therefore sought to confirm that anaphase I failure and ongoing proteolysis were co-existing within the same oocytes. To do this, we monitored securin-GFP while simultaneously imaging spindles and chromosomes in the same oocytes. We found that securin-GFP levels increased during the first 5-6 h post-GVBD, coincident with bipolar spindle assembly and chromosome alignment in both Cep55- and mock-depleted oocytes (Fig. 3G). Although proteolysis then occurred in both controls and Cep55-depleted oocytes, chromosome separation occurred in the former but not the latter (Fig. 3G; Movies 3 and 4). We repeated these experiments using cyclin B1-GFP instead of securin-GFP and obtained identical results (Fig. S2; Movies 5 and 6). Thus, following Cep55 depletion, anaphase I does not occur despite normal SAC inactivation and intact proteolysis, showing that anaphase I is not exclusively driven by proteolysis in oocytes.

Metaphase I arrest is due to reduced Cdk1 phosphoinhibition

Separase activity is modulated by securin as well as Cdk1 activity levels (Stemmann et al., 2001). Because securin destruction

Journal of Cell Science (2019) 132, jcs233379. doi:10.1242/jcs.233379

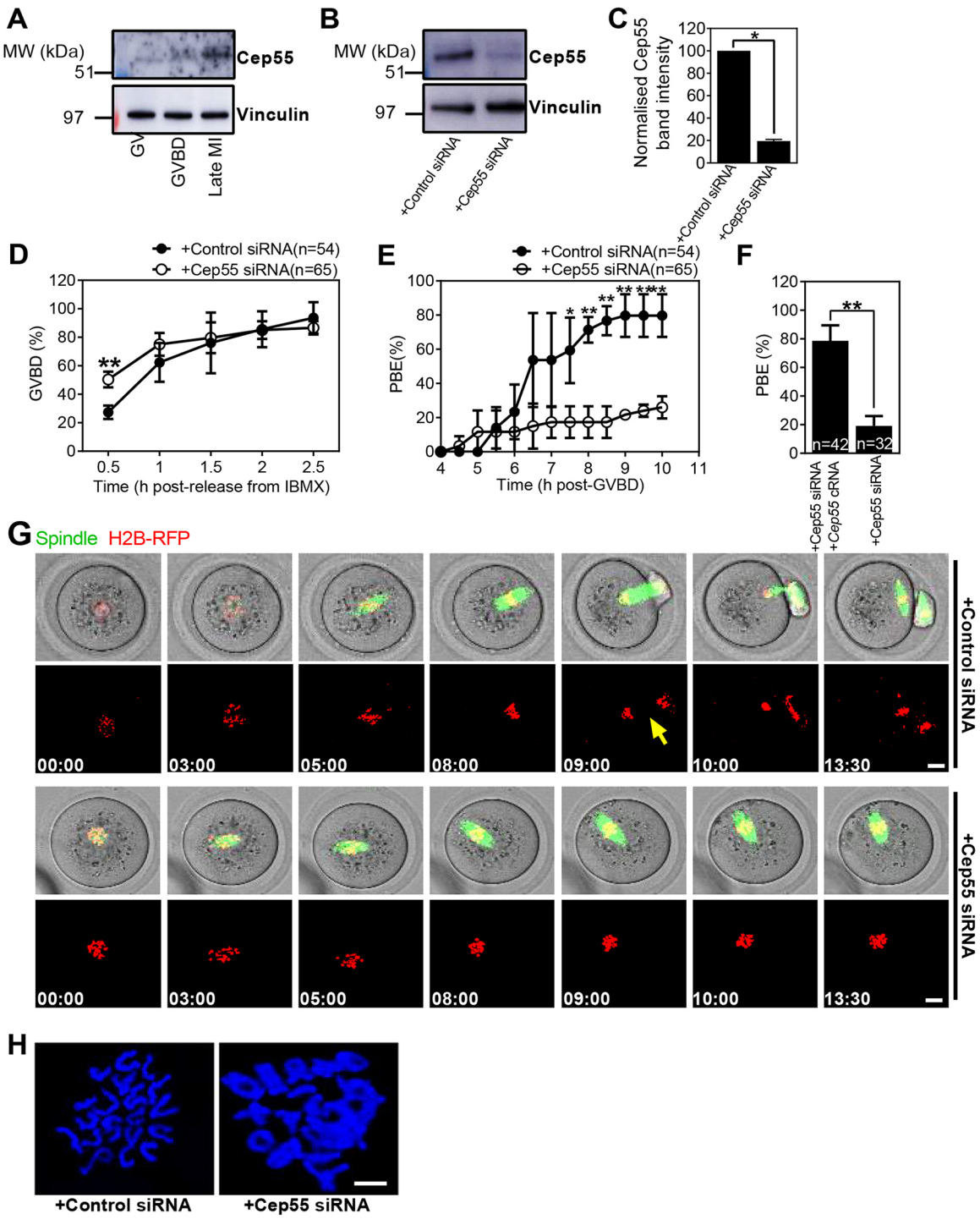

Fig. 1. Cep55 depletion inhibits anaphase I. (A) Samples (50 oocytes) at the GV stage, GVBD and late MI (7 h post-GVBD) were immunoblotted for Cep55 and vinculin. Cep55 levels were low at GV and GVBD, but increased markedly by late MI. (B) Samples (50 oocytes) of Cep55-specific siRNA-injected oocytes were immunoblotted along with control siRNA-injected (mock-depleted) oocytes at 7 h post-GVBD for Cep55 and vinculin. (C) Band intensities of Cep55 on blot were quantified and normalised to values found in controls. (D,E) Rates of GVBD and polar body extrusion (PBE) in mock- and Cep55-depleted oocytes. Oocyte numbers are shown in parentheses. (F) PBE rates in Cep55-depleted oocytes with or without co-expression of Cep55 from injected Cep55 cRNA. PBE rates were determined at 20 h post-GVBD. (G) Representative timelapse images of spindles and chromosomes in live mock-depleted (*n*=54 oocytes) and Cep55-depleted (*n*=65 oocytes) oocytes during MI (see Movies 1 and 2). Yellow arrow indicates anaphase. Time is hh:mm post-GVBD. Scale bars: 10 µm. (H) Chromosome spreads from mock- and Cep55-depleted oocytes prepared at 20 h post-GVBD. Graphs show mean±s.e.m. **P*<0.05, ***P*<0.01 (two-tailed Student's *t*-test). Results are representative of at least three independent experiments. Scale bar: 5 µm.

occurred normally after Cep55 depletion (Fig. 3), we reasoned that Cdk1 inactivation might be perturbed. Strikingly, we found that Cdk1 activity remained markedly higher in late MI following Cep55 knockdown compared with controls (Fig. 4A,B). Because sustained Cdk1 activity was not a result of failed cyclin B1 destruction (Fig. S2), we next investigated whether the other mechanism for inactivating

Journal of Cell Science (2019) 132, jcs233379. doi:10.1242/jcs.233379

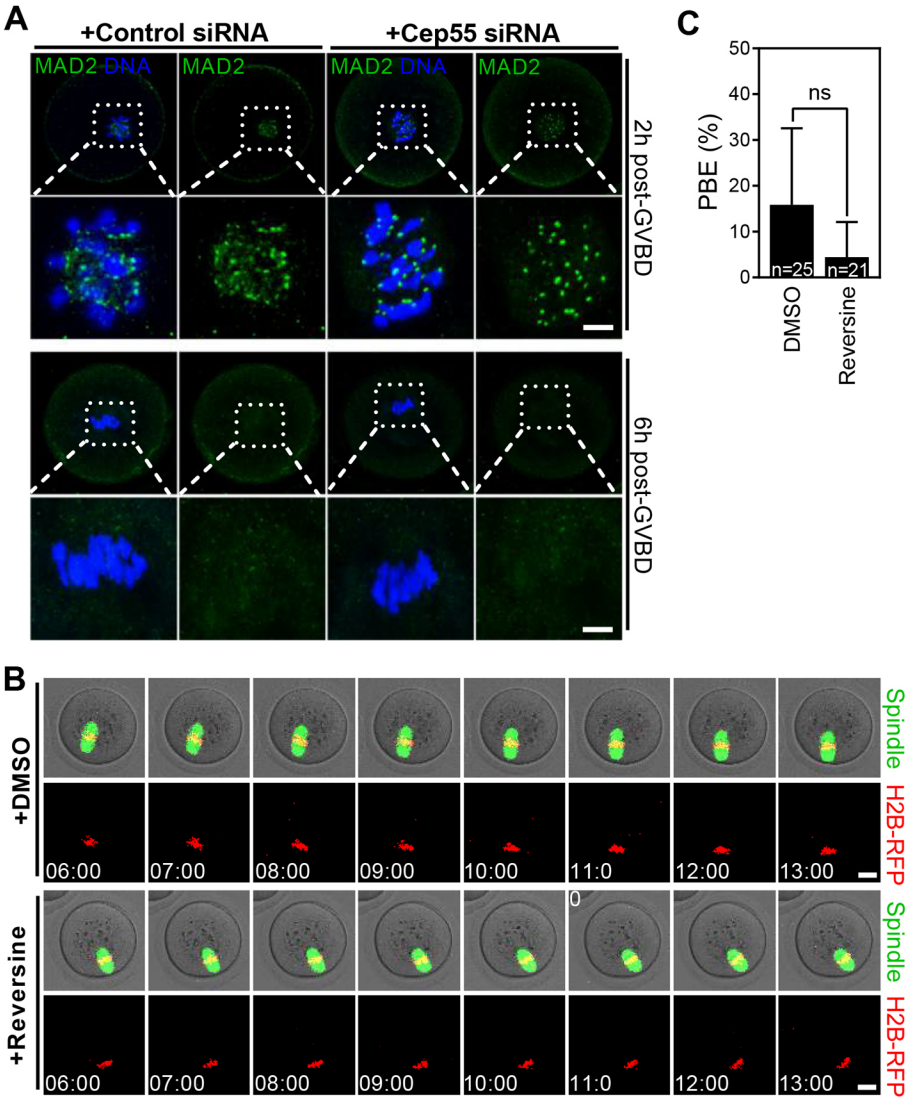

Fig. 2. SAC activation is not responsible for MI arrest in Cep55-depleted oocytes. (A) Representative images of oocytes immunostained for MAD2 and chromosomes. Note the high levels of MAD2 associated with chromosomes in early MI (2 h post-GVBD) when kinetochores are mostly unattached in oocytes. In contrast, by 6 h post-GVBD when kinetochores have acquired bipolar attachments leading to chromosome alignment and stretching, MAD2 levels on chromosomes had dissipated in both mock- and Cep55-depleted oocytes, consistent with SAC inactivation (n>20 per group). Scale bar: 5 µm. (B) Images of spindles and chromosomes from representative timelapse series of Cep55-depleted oocytes treated with either DMSO solvent or the Mps1 inhibitor, reversine. Scale bars: 10 µm. (C) PBE rates in control and reversine-treated Cep55-depleted oocytes. Note that neither treatment induces anaphase I nor PBE and that PBE rates remain low in both groups. Time is hh:mm post-GVBD. Data are mean±s.e.m. ns, not significant (Student's t-test). Results are representative of at least three independent experiments.

Cdk1, inhibitory Tyr15 phosphorylation (pY15), was affected. Significantly, we found that levels of pY15-phosphorylated Cdk1 (p-Cdk1) in late MI were dramatically reduced after Cep55 knockdown compared with controls (Fig. 4C,D).

These data suggested that anaphase I was being prevented by persistent Cdk1 activity brought about by suboptimal inhibitory phosphorylation. If this were the case, then forcing Cdk1 inactivation should induce anaphase I. We therefore treated MI-arrested Cep55 knockdown oocytes with the small molecule Cdk1 inhibitor, flavopiridol (Wei et al., 2018). Significantly, flavopiridol induced anaphase I and PBE in >70% of Cep55-depleted oocytes compared with only 20% after DMSO treatment (Fig. 4E,F; Movies 7 and 8).

Thus, persistent Cdk1 activity and reduced Cdk1 phosphoinhibition are associated with metaphase I arrest after Cep55 knockdown, and forced Cdk1 inactivation over-rides this arrest to induce anaphase I. Significantly, this pathway is not under SAC control, as reversine could not overcome metaphase I arrest (Fig. 2B,C).

Reduced Cdc25 activity promotes phosphoinhibition in late MI

The need for Cdk1 phosphoinhibition to inactivate Cdk1 sufficiently for anaphase I initiation was unexpected, as it is widely believed that cyclin B1 destruction is sufficient (Herbert et al., 2003). Further supporting a role for phosphoinhibition, p-Cdk1 levels exhibited a prominent rise specifically in late MI in untreated oocytes (Fig. 5A). Somewhat surprisingly, levels of Wee1B kinase, which mediates inhibitory Cdk1 phosphorylation (Oh et al., 2011), did not increase by late MI; however, levels of Cdc25B phosphatase, which removes Wee1B-induced inhibitory phosphorylation (Adhikari and Liu, 2014), decreased concurrently with increased p-Cdk1 (Fig. 5A). Taken together, these data suggest that anaphase I requires Wee1B-dependent Cdk1 phosphoinhibition secondary to reduced phosphatase activity, rather than to increased inhibitory kinase activity.

If inhibitory phosphorylation is required for Cdk1 inactivation during late MI, then disrupting Wee1B in late MI should compromise MI exit. Because Wee1B regulates Cdk1 during G2 arrest (Han et al., 2005), we avoided approaches (e.g. knockdown) that would disrupt Wee1B from the GV stage to avoid incurring early-stage defects that could impact late MI events. Instead, we used small molecule inhibitors that could be introduced specifically in late MI. We treated oocytes at 5 h post-GVBD with either the Wee1-specific inhibitor MK1775 (Strauss et al., 2018) or DMSO solvent. Timelapse imaging showed that 70-80% of DMSO-treated oocytes underwent anaphase I followed by

Journal of Cell Science (2019) 132, jcs233379. doi:10.1242/jcs.233379

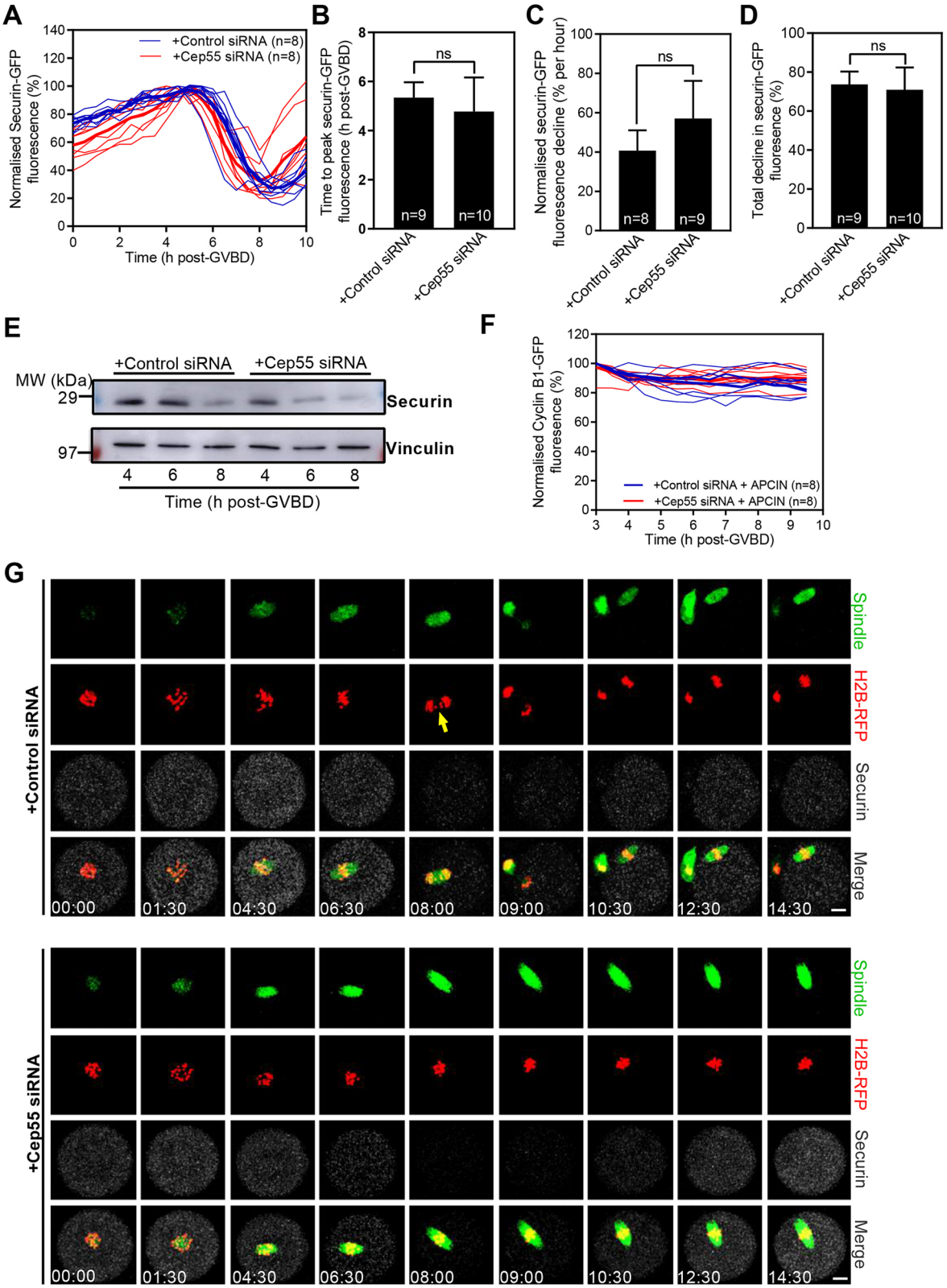

Fig. 3. Anaphase I failure following Cep55 depletion despite intact proteolysis. (A) Timelapse fluorescence profiles of securin-GFP in mock- and Cep55-depleted oocytes. Bold lines are means; traces of individual oocytes are indicated by fine lines. Oocyte numbers are shown in parentheses. (B-D) Time taken to attain peak securin-GFP fluorescence (B), rate of fluorescence decline (C) and the total fluorescence decline (D) in mock- and Cep55-depleted oocytes. Data are mean±s.e.m. ns, no significant difference (P>0.05), two-tailed Student's t-test. (E) Changes in endogenous securin levels during MI in mock- and Cep55-depleted oocytes (n=50 oocytes per lane). (F) Timelapse fluorescence profiles of cyclin B1-GFP in APCIN-treated mock- and Cep55-depleted oocytes. Bold lines are means; traces of individual oocytes are indicated by fine lines. Oocyte numbers are shown in parentheses. (G) Representative timelapse images of spindles, chromosomes and securin-GFP in live mock-depleted (n=8 oocytes) and Cep55-depleted (n=8 oocytes) oocytes during MI (see Movies 3 and 4). Yellow arrow indicates anaphase. Time is hh:mm post-GVBD. Scale bars: 10 µm. Results are representative of at least three independent experiments.

Journal of Cell Science (2019) 132, jcs233379. doi:10.1242/jcs.233379

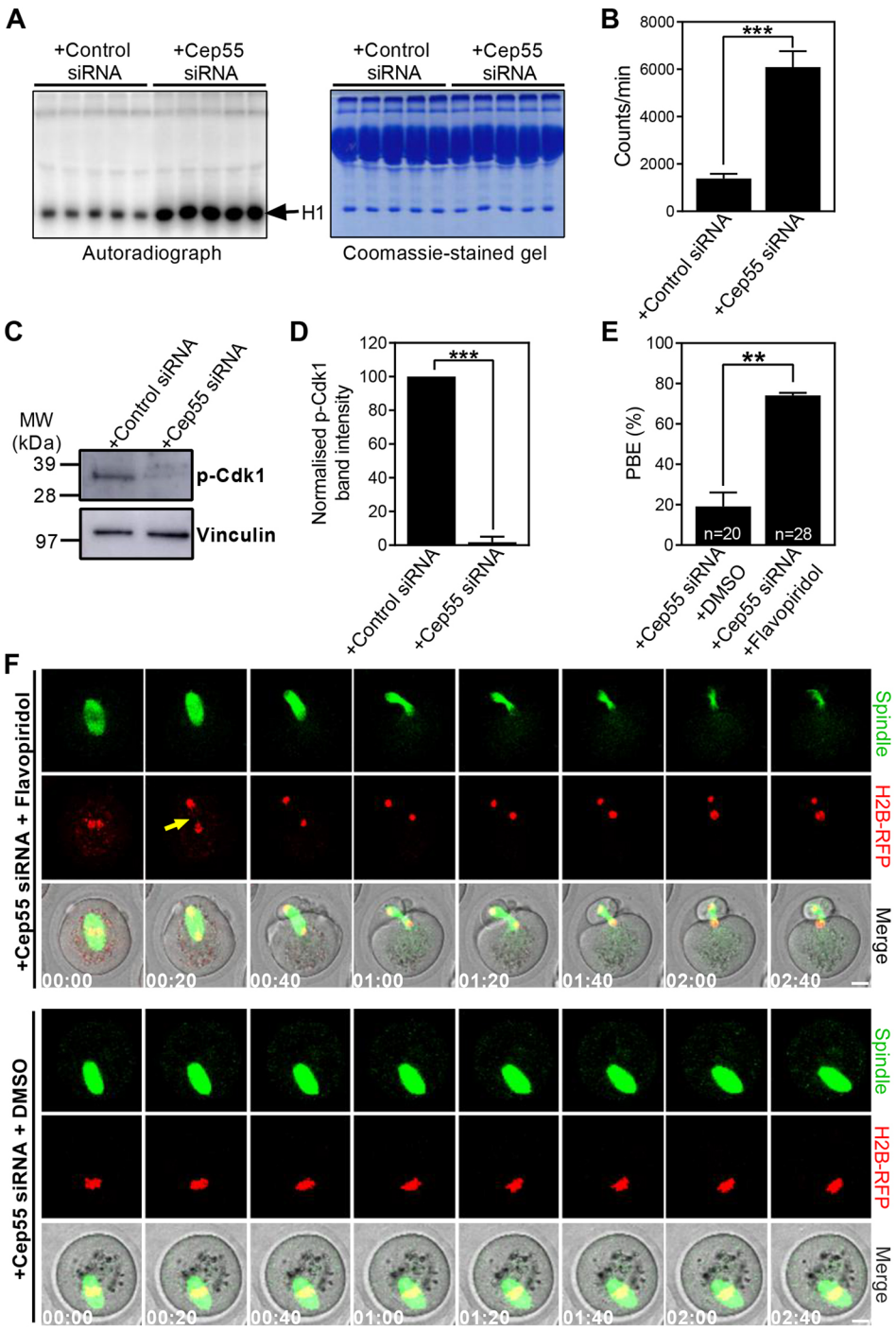

Fig. 4. Sustained Cdk1 activity prevents anaphase I in Cep55-depleted oocytes. (A) Cdk1-dependent *in vitro* phosphorylation of histone H1 (H1) in mock- and Cep55-depleted late MI (7 h post-GVBD) single oocytes (Autoradiograph). The gel stained with Coomassie Blue shows equal loading of lysate and H1 substrate (n=5 independent reactions per condition). (B) Mean H1 kinase assay radioactivity in mock- and Cep55-depleted oocytes. (C) Tyr15 phosphorylated Cdk1 (p-Cdk1) levels in mock- and Cep55-depleted oocytes in late MI (7 h post-GVBD); n=50 oocytes per lane. (D) Average p-Cdk1 band intensity from three experiments as described in C. (E) PBE rates following treatment of MI-arrested Cep55-depleted oocytes with either DMSO or flavopiridol. PBE rates were determined at 14 h post-GVBD. (F) Representative timelapse images of spindles and chromosomes in live MI-arrested Cep55-depleted oocytes following treatment with either DMSO or flavopiridol (see Movies 7 and 8). Yellow arrow indicates anaphase. Time is hh:mm post-GVBD. Scale bars: 10 µm. Graphs show mean±s.e.m. $^{**}P<0.01$, $^{***}P<0.001$ (two-tailed Student's t-test). Results are representative of at least three independent experiments.

PBE by 9-10 h post-GVBD, as before (Fig. 5B,C; Movie 9). Strikingly, >90% of MK1775-treated oocytes failed to undergo either anaphase I or PBE, even by 15 h post-GVBD (Fig. 5B,C and Movie 10). Thus, inhibition of Wee1B specifically in late MI prevented anaphase I.

We reasoned that Cep55 depletion could lead to reduced p-Cdk1 levels in late MI by causing a shift from a normal Cdc25B-suppressed state to relative Cdc25B overactivity. If so, then reducing Cdc25B activity in Cep55-depleted oocytes during late MI should restore the balance and promote anaphase I. To test this, we treated Cep55-depleted oocytes with a specific Cdc25 inhibitor, NSC95397, late in MI. As validation of NSC95397, we found that (at the dose used) GVBD was significantly reduced and p-Cdk1 levels increased, proving efficient phosphatase inhibition (Fig. S3). Strikingly, inhibiting Cdc25 using NSC95397 induced anaphase I in ∼70% of Cep55-depleted oocytes compared with only ∼20% following DMSO treatment (Fig. 5D,E; Movies 11 and 12).

Next, we asked whether changes in Cdc25B protein abundance might account for altered activity following Cep55 depletion. Notably, accompanying the reduction in p-Cdk1 following Cep55 depletion, we found that Cdc25B underwent a marked increase whereas Wee1B was unaffected (Fig. 5F,G). Thus, loss of Cep55 promoted Cdc25B stability in late MI that resulted in sustained Cdk1 activity and anaphase I failure.

Journal of Cell Science (2019) 132, jcs233379. doi:10.1242/jcs.233379

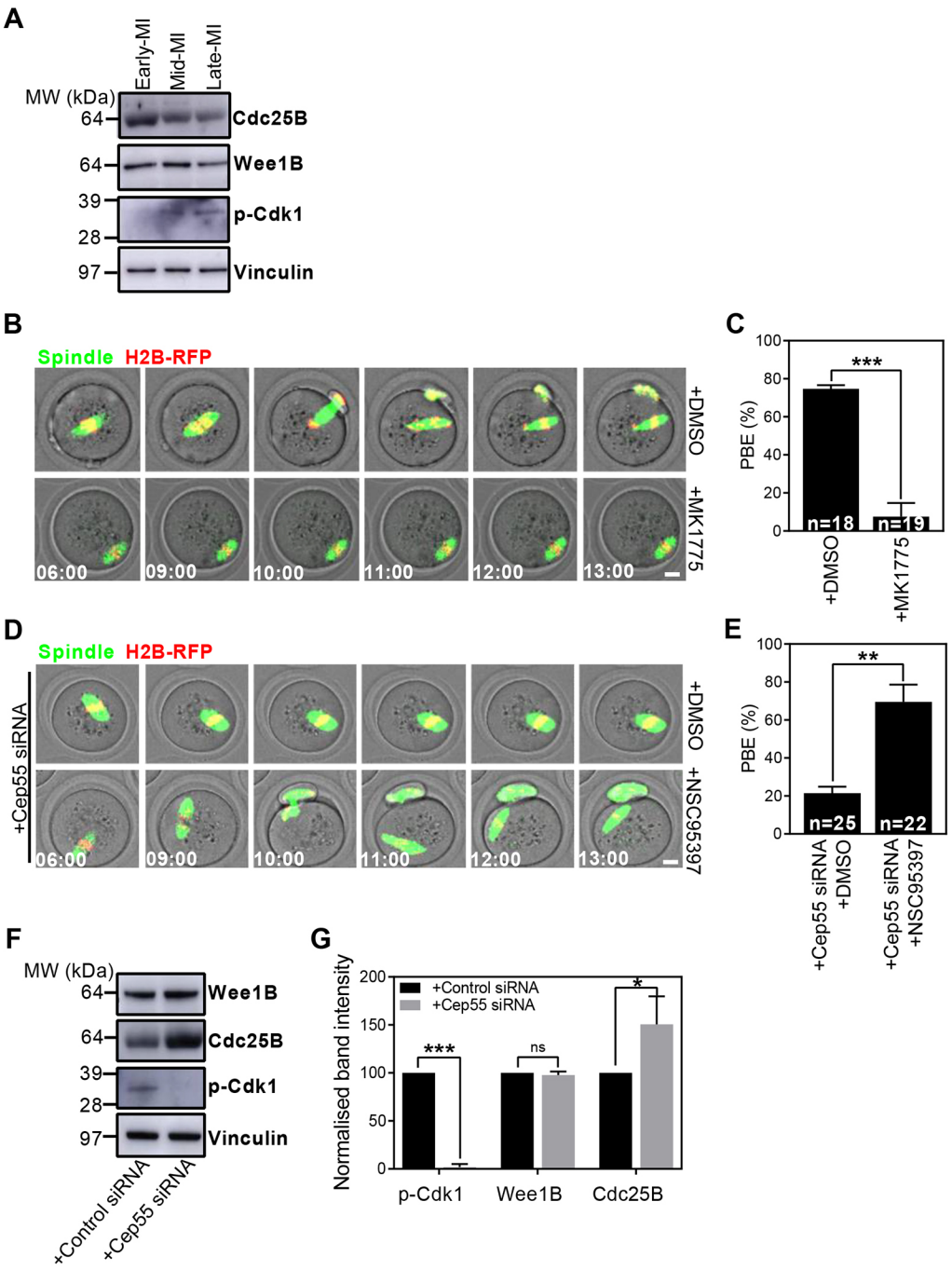

Fig. 5. Sustained Cdk1 activity is caused by Cdc25 phosphatase overactivity. (A) Endogenous levels of Cdc25B, Wee1B and p-Cdk1 at 3 h (early MI), 5 h (mid-MI) and 7 h post-GVBD (late MI); *n*=30 oocytes per lane. (B) Representative timelapse images of spindles and chromosomes in live oocytes treated with either DMSO or with the Wee1 inhibitor MK1775 (see Movies 9 and 10). Time is hh:mm post-GVBD. Scale bar: 10 µm. (C) PBE rates in oocytes treated with either DMSO or MK1775 determined at 14 h post-GVBD. (D) Representative timelapse images of spindles and chromosomes in live Cep55-depleted oocytes treated with either DMSO or the Cdc25B inhibitor NSC95397 at 6 h post-GVBD (see Movies 11 and 12). Time is hh:mm post-GVBD. Scale bar: 10 µm. (E) PBE rates in Cep55-depleted oocytes treated with either DMSO or NSC95397 determined at 14 h post-GVBD. (F) Levels of Wee1B, Cdc25B and p-Cdk1 in mock- and Cep55-depleted oocytes in late MI (7 h post-GVBD). (G) Normalised band intensities for Wee1B, Cdc25B and p-Cdk1 in mock- and Cep55-depleted oocytes in late MI. Graphs show mean±s.e.m. **P*<0.05; ***P*<0.01; ****P*<0.001; ns, not significant (two tailed Student's *t*-test). Results are representative of at least three independent experiments.

We then asked whether overexpression of Cep55 would have the opposite effect to Cep55 depletion and lead to accelerated exit from MI. This was not the case, as the timings of anaphase I and PBE were completely unaffected when Cep55 was overexpressed from microinjected cRNA (Fig. S4), suggesting that phosphorylation-dependent pathways are not sufficient for driving exit events independently of proteolysis. We wondered whether Cep55 might influence Cdc25B stability through direct binding. This did not appear to be the case because Cdc25B exhibited diffuse cytoplasmic localisation (Fig. S5A), similar to previous findings (Oh et al., 2010), that was distinct from the Cep55 enrichment at spindle poles seen during both MI and MII (Fig. S1). Furthermore, Cep55 levels increased even further by MII without an accompanying decrease in Cdc25B (Fig. S5B). Together, these data suggest that the effect of Cep55 on Cdc25B is complex and might be restricted to a narrow window in late MI.

DISCUSSION

MI in oocytes is known to be prone to chromosome mis-segregation. Here, we show that Cdk1 phosphoinhibition secondary to Cdc25 suppression is necessary for initiating anaphase I in oocytes, independently of proteolysis. Because phosphoinhibition was not under control of the SAC in oocytes (Fig. 2B,C), these data show that anaphase I in oocytes is not exclusively regulated by proteolysis and, hence, by the SAC. Moreover, because the status of kinetochore-microtubule attachment/tension is relayed by the SAC, the timing of

Journal of Cell Science (2019) 132, jcs233379. doi:10.1242/jcs.233379

phosphoinhibition is not coordinated with chromosome alignment, rendering chromosome segregation at increased risk of going awry in oocytes. Our findings differ from previous reports linking inhibitory Cdk1 phosphorylation with exit from M phase because, in these cases, proteolysis was also impacted (D'Angiolella et al., 2007; Forester et al., 2007; Oh et al., 2011).

In contrast to the role of Cep55 in abscission, long after anaphase in mitosis (Fabbro et al., 2005; Zhao et al., 2006), in female MI, Cep55 is required to initiate anaphase I by destabilising Cdc25B to promote Cdk1 inactivation. Cep55 appears to subdue Cdk1 in other situations, as Cdk1 is prematurely activated in breast cancer cells lacking Cep55 that are treated with anti-mitotic agents (Kalimutho et al., 2018). Furthermore, we observed that, although the overall capacity to enter M phase (marked by GVBD) was unchanged by Cep55 depletion, there was a doubling of GVBD rates within the first 30 min after release from IBMX (Fig. 1D), consistent with accelerated Cdk1 activation. We do not currently know the mechanism by which Cep55 induces Cdc25B instability in late MI. It may not be by direct binding, based on the lack of colocalisation in oocytes and our unpublished immunoprecipitation work involving somatic cells. Interestingly, destruction of Cdc25B mediated by the β-TrCP-Skp1-Cul1-F-box (SCF) E3 ubiquitin ligase occurs at the metaphase-to-anaphase transition during mitosis (Thomas et al., 2010). One possibility is that Cep55 might promote Cdc25B-SCF interaction either directly or indirectly in late MI when Cep55 levels are maximal. Phosphorylation pathways do not appear to be sufficient to induce MI exit without additional input from proteolysis because Cep55 overexpression did not accelerate MI exit. Additionally, because Cep55 levels continued to increase into MII without a concomitant decrease in Cdc25B, there is probably an additional regulatory layer that limits the effects of Cep55 to late MI; perhaps the unique MII environment involving cytostatic factors has some role to play, but this remains to be investigated.

Our findings are consistent with a previous report showing that MI is disrupted following Cep55 depletion in oocytes (Xu et al., 2015). However, using oocytes that were fixed and immunostained at a single timepoint, that study suggested that Cep55 depletion induced spindle and chromosome alignment defects (Xu et al., 2015). Significantly, the impact of Cep55 depletion on GVBD (Fig. 1D, first 30 min) was not previously identified, and single-timepoint analyses were performed relative to time of transfer to IBMX-free medium rather than relative to GVBD (Xu et al., 2015), risking comparing oocytes at very different stages of MI. Here, using Cep55-specific siRNA sequences previously characterised in murine cells (Kalimutho et al., 2018) and extensive analyses of live oocytes (Fig. 1G, Fig. 3G, Fig. 4F, Fig. 5D) in addition to fixed oocytes (Fig. S1) in strict relationship to GVBD, we showed that spindle assembly and chromosome alignment remain intact following Cep55 depletion. Moreover, entirely in keeping with unperturbed attainment of metaphase I, we showed that SAC silencing occurs normally, as does APC-Cdc20-mediated proteolysis.

Surprisingly, the full extent of proteolysis that typically occurs during late MI was not sufficient to induce the degree of Cdk1 inactivation necessary for anaphase I, contrasting sharply with mitosis, in which anaphase requires only a fraction of cyclin B1 to be destroyed (Wolf et al., 2007, 2006). This could be related to cyclin B1 being present in large excess (~sixfold) over Cdk1 in oocytes (Levasseur et al., 2019) versus the reverse in somatic cells (30-fold excess Cdk1 over cyclin B1) (Arooz et al., 2000). Under these conditions in oocytes, sufficient cyclin B1 might remain after proteolysis is complete to maintain Cdk1 above the threshold required for separase activation, necessitating Cep55-dependent phosphoinhibition.

MATERIALS AND METHODS

Oocyte collection, culture and microinjection

All animals were housed in a specific pathogen-free environment in filter-top cages and fed a standard diet. All work involving animals complied with all relevant ethical regulations and was approved by the Animal Ethics Committee at the University of Queensland.

Oocytes were isolated from the ovaries of 3- to 4-week-old B6CBAF1 female mice 44–46 h after intraperitoneal injection of 7.5 international units (IU) of pregnant mare serum gonadotrophin (Pacific vet). Dissected ovaries were immediately transferred to the laboratory in prewarmed αMEM HEPES-buffered medium (Sigma-Aldrich) containing 50 µM 3-isobutyl-1-methylxanthine (IBMX; Sigma-Aldrich), which prevents oocytes from undergoing GVBD (Gui and Homer, 2012, 2013; Homer et al., 2009; Wei et al., 2018). Ovarian antral follicles were punctured in IBMX-treated medium in 35×10 mm^2 dishes using a 27G needle under direct vision on the stage of a stereomicroscope (M165C, Leica Microsystems). Only fully-grown cumulus-covered oocytes were isolated and used for further experiments. For longer-term culture and for all confocal imaging, oocytes were cultured in microdrops of M16 media (Sigma-Aldrich) under embryo-tested light mineral oil (Sigma-Aldrich) at 37°C in an atmosphere of 5% CO_2 in air (Gui and Homer, 2012, 2013; Homer et al., 2009, 2005b; Wei et al., 2018).

For microinjection (Gui and Homer, 2012, 2013; Homer et al., 2009; Wei et al., 2018), GV-stage oocytes in IBMX-treated medium were stabilised using suction applied through a hydraulic syringe to a prefabricated holding pipette (inner diameter 15 µm, outer diameter 75 µm, 35° bend; The Pipette Company). Microinjection needles were pulled from capillary tubes (0.86 mm inner diameter, 1.5 mm outer diameter; Harvard Apparatus) to a predetermined calibre using a vertical pipette puller (P30 vertical micropipette puller, Sutter Instruments). The tip of the microinjection pipette was advanced across the zona pellucida and oolemma into the cytoplasm of the oocyte, aided by a brief electrical pulse delivered by an intracellular electrometer (IE-25IA, Warner Instruments). A precise volume of test solution roughly equal to 5% of the oocyte volume was then delivered to the oocyte using a Pneumatic PicoPump (PV-820, World Precision Instruments). The rate of oocyte death following microinjection was consistently <10%.

cRNA constructs and siRNA

The mMESSAGE mMACHINE High Yield Capped RNA Transcription Kit (Ambion) was used to produce cRNA constructs by T3 promoter-driven *in vitro* transcription from linearised DNA templates (Gui and Homer, 2012, 2013; Homer et al., 2009, 2005b; Wei et al., 2018). Constructs used in this paper were histone 2B (H2B)-RFP, securin-GFP, cyclin B1-GFP and full-length murine Cep55 cRNAs. The latter was siRNA-resistant by virtue of lacking the 5′UTR targeted by the siRNA (see below). All plasmids were fully sequenced prior to transcription. Following *in vitro* transcription, cRNA size was verified on agarose gels and concentrations were determined using a spectrophotometer. Constructs were microinjected at the following concentrations: H2B-RFP at 250 ng $µl^{-1}$, securin-GFP at 200 ng $µl^{-1}$, cyclin B1-GFP at 200 ng $µl^{-1}$ and Cep55 at 1.5 µg $µl^{-1}$. Following microinjection at the GV stage, oocytes were held in 50 µM IBMX for at least 2 h to allow time for protein translation while maintaining GV arrest. Oocytes were then washed through 5-6 drops of IBMX-free media to allow resumption of maturation.

For depleting Cep55, GV-stage oocytes were microinjected with a previously published siRNA sequence that was designed to target the 5′UTR of murine Cep55: 5′-AGCUACUGAGCAGUAAGCAAACAT T-3′; 5′-AAUGUUUGCUUACUGCUCAGUAGCUUU-3′; control siRNA sequences were 5′-UUCUUCGAACGUGUCACGUTT-3′ and 5′-ACGUGACACGUUCGGAGAATT-3′ (Gene Pharma, Shanghai, China) (Kalimutho et al., 2018). All siRNAs were injected at a final needle concentration of 100 µM. Following microinjection, oocytes were maintained in IBMX-treated medium for 24 h to allow time for protein knockdown.

Drugs and chemicals

Stock solutions of all small molecule inhibitors were made in DMSO at the highest possible concentration that enabled complete solubilisation, thereby minimising the volume of DMSO added to media. For inhibiting Cdk1 activity, flavopiridol (SelleckChem; 10 mM stock solution) was dissolved in medium for a final concentration of 5 µM, as used previously in mouse oocytes (Wei et al., 2018). The APC-Cdc20-specific inhibitor APCIN (Sigma-Aldrich; 50 mM stock solution) (Sackton et al., 2014; Wei et al., 2018) was used at 150 µM to inhibit proteolysis at 4 h post-GVBD before proteolysis had begun. To inhibit Wee1B activity late in MI (5-6 h post-GVBD), MK1775 (Strauss et al., 2018) (Celleckchem; 10 mM stock solution) was used at a concentration of 5 µM. To inhibit Cdc25B activity late in MI (5-6 h post-GVBD), NSC95397 (Cayman Chemical, USA; 10 mM stock solution) was used at a concentration of 400 nM after validation (see Fig. S3). As a control, DMSO, which was used to dissolve all inhibitors, was added to media at a final concentration that was the same concentration attained when inhibitors were added.

Histone H1 kinase assay

Individual oocytes were collected into tubes and immediately frozen on dry ice and stored at −80°C until lysis. Oocytes were lysed by four freeze-thaw cycles in 2 µl of 20 ng µl^{-1} BSA in water. Assay buffer (8 µl; 50 mM β-glycerophosphate pH 7.35, 1.5 mM EGTA, 1 mM DTT and 10 mM MgCl2) was added and samples were prewarmed to 37°C. Unlabelled ATP, histone H1 (Sigma-Aldrich) and γP32 ATP (3000 µCi mmol^{-1}; Perkin Elmer) were mastermixed and added such that each reaction contained 1 µg of H1, 10 µCi of γP32 ATP and 5 µM unlabelled ATP in a final volume of 12 µl. Reactions were incubated for 70 min at 37°C and terminated by denaturation in SDS-PAGE loading buffer. Samples were resolved by SDS-PAGE and gels were stained with Coomassie Blue and vacuum dried. Exposures were collected using a phosphor storage screen. Kinase activity was quantified by scintillation counting excised gel pieces in Ultima Gold scintillant on a Packard Tri-Carb beta counter.

Immunoblotting

Western blotting was performed as described previously (Gui and Homer, 2012, 2013; Homer et al., 2009; Wei et al., 2018). Protein samples were prepared by washing oocytes with ultrapure water and lysing in LDS sample buffer (NuPAGE, Invitrogen). Samples were vigorously agitated and immediately snap-frozen at −80°C for storage until required. Samples were boiled at 95°C for 5 min following addition of reducing agent (NuPAGE, Invitrogen). Proteins were separated on 4-12% Bis-Tris gels (NuPAGE; Invitrogen Australia) and transferred to PVDF membranes (Immobilon-P, Millipore). Following transfer, membranes were blocked for 1 h at room temperature in 3% BSA in TBS (25 mM Trizma base, 150 mM sodium chloride) containing 0.05% Tween-20 (TBST). Primary antibody incubation was carried out overnight at 4°C in blocking buffer. The primary antibodies used were Cep55 [1:2000, made by the Khanna laboratory and described previously (Kalimutho et al., 2018)], Wee1B [1:800; a very kind gift from Marco Conti (Oh et al., 2011)], Cdc25B (New England Biolabs 9525#, 1:1000), securin (Abcam-ab3305; 1:1000), p-Cdk1 (Cell Signalling-9111S; 1:1000) and vinculin (Sigma Aldrich-V9131; 1:2000). Following three 5 min washes in TBST, membranes were incubated in the appropriate HRP-conjugated goat anti-rabbit or goat anti-mouse secondary antibodies (1:1000; Bio-Rad) for 1 h at room temperature. Chemiluminescence detection was performed using Western Lightning ECL-Pro (Perkin Elmer) and imaged using Image Quant LAS500 (GE Healthcare).

Immunofluorescence staining

Oocytes were fixed and stained as described previously (Gui and Homer, 2012, 2013; Homer et al., 2009). Briefly, oocytes were washed in PHEM buffer (pH 7.0) and prepermeabilised in 0.25% Triton-X in PHEM. Oocytes were then fixed in 3.7% paraformaldehyde solution in PHEM for 20 min. Oocytes were blocked overnight in 3% BSA in PBS containing 0.05% Tween-20 at 4°C. Primary antibody incubation with anti-Cep55 antibody (1:200) was carried out for 1 h at 37°C. Primary antibody incubation with anti-MAD2 antibody (1:200) was carried out for 4 h at 37°C. Following three 5 min washes in PBS containing 0.5% BSA and 0.05% Tween-20, oocytes were incubated with the appropriate Alexa Fluor 488-conjugated secondary antibodies (1:200; ThermoFisher) for 1 h at 37°C. Oocytes were then washed three times before staining for DNA by incubating in Hoechst 33342 (10 µg ml^{-1}; Sigma) for 5 min.

Confocal microscopy

Imaging was performed using a Leica TCS SP8 confocal microscope equipped with a 20×0.75 NA Apochromat water-immersion objective fitted with an automated pump cap (water immersion microdispenser, Leica; automated pump mp-x controller, Bartels Mikrotechnik) as described previously (Wei et al., 2018).

Timelapse microscopy was used to image spindles and chromosomes simultaneously (Wei et al., 2018). To visualise microtubules, silicon rhodamine (SiR)-Tubulin dye (Cytoskeleton, Denver, CO) (Lukinavičius et al., 2014) was added to media at a final concentration of 100 nM, as validated previously in mouse oocytes (Wei et al., 2018). Oocytes were imaged in 1-2 µl microdrops of M16 medium in glass-bottom dishes (35×10 mm dish; MatTek) under mineral oil enclosed within a purpose-built stage-mounted incubation chamber designed to maintain conditions of 37°C and 5% CO_2 in air. Temperature fluctuation was further buffered by enclosing the entire microscope, including the stage-mounted chamber, in a custom-designed polycarbonate incubator (Life Imaging Services) that maintained a stable internal temperature of 37°C. Automated image capture was driven by the Leica LAS X software. At the commencement of imaging, the positions of the oocytes in the *z*-axis were located. The complete stack was then derived by setting a stack thickness of 50 µm. Z-stacks were acquired with step intervals of 4 µm at 5 min (Flavopiridol treatment), 10 min (for securin-GFP and cyclin B1-GFP destruction measurement) or 30 min (all other experiments) intervals and a speed of 600 Hz. Using the Leica mark-and-find tool, we typically imaged multiple groups of oocytes in separate droplets in each experiment. The 561 nm (for H2B-RFP) and 633 nm (for SiR-Tubulin) laser lines were used at 0.5% and 3% intensity, respectively.

Post-acquisition image processing was performed using Leica LAS X software and images were assembled into panels using Adobe Illustrator (Adobe Systems). Fluorescence images were produced by Z-projecting the entire stack of fluorescence images from both channels and merging them with images in the bright-field channel.

For quantifying proteolysis, GV-stage oocytes were microinjected with securin-GFP or cyclin B1-GFP cRNA and allowed to express protein for at least 2 h while being maintained GV-arrested using IBMX. GFP fluorescence was detected using the 488 nm laser line at 1% intensity. Z-stacks of 50 µm thickness were acquired with step intervals of 5 µm at 30 min intervals at a speed of 600 Hz. After importing LAS X images into Image J software (NIH, Bethesda, MD), a maximum intensity projection of the entire Z-stack was performed, a region of interest was drawn around the entire oocyte and the fluorescence intensity within this area was measured over time. Graphs of fluorescence intensity against time were then normalised and plotted.

Graphical representation and statistical analysis

GraphPad Prism (GraphPad, USA) was used to calculate the mean and standard error of the mean (s.e.m.). Statistical comparisons were made using a two-tailed Student's *t*-test with Welch's correction. Graphs were prepared in GraphPad Prism. *P* values were represented as $*P<0.05$, $**P<0.01$, $***P<0.001$; ns denotes $P>0.05$ (not significant). All experiments were repeated a minimum of three times.

Acknowledgements

We are very grateful to Marco Conti (University of California, San Francisco, CA, USA) for the very kind gift of anti-Wee1B antibody.

Competing interests

The authors declare no competing or financial interests.

Author contributions

Methodology: C.Z., J.L.H.; Validation: C.Z.; Formal analysis: H.A.H.; Investigation: C.Z., H.A.H.; Data curation: C.Z., J.L.H.; Writing - original draft: H.A.H.; Writing - review & editing: H.A.H.; Visualization: C.Z.; Supervision: K.K.K., H.A.H.; Project administration: C.Z., H.A.H.; Funding acquisition: H.A.H.

Funding
This work was funded by the Professor Christopher Chen Endowment Fund, Start-up funding from the Faculty of Medicine, University of Queensland and National Health and Medical Research Council Project Grants (APP1078134 and APP1103689) to H.A.H.

Supplementary information
Supplementary information available online at
http://jcs.biologists.org/lookup/doi/10.1242/jcs.233379.supplemental

References

Adhikari, D. and Liu, K. (2014). The regulation of maturation promoting factor during prophase I arrest and meiotic entry in mammalian oocytes. *Mol. Cell. Endocrinol.* **382**, 480-487. doi:10.1016/j.mce.2013.07.027
Arooz, T., Yam, C. H., Siu, W. Y., Lau, A., Li, K. K. W. and Poon, R. Y. C. (2000). On the concentrations of cyclins and cyclin-dependent kinases in extracts of cultured human cells. *Biochemistry* **39**, 9494-9501. doi:10.1021/bi0009643
D'angiolella, V., Palazzo, L., Santarpia, C., Costanzo, V. and Grieco, D. (2007). Role for non-proteolytic control of M-phase-promoting factor activity at M-phase exit. *PLoS ONE* **2**, e247. doi:10.1371/journal.pone.0000247
Fabbro, M., Zhou, B.-B., Takahashi, M., Sarcevic, B., Lal, P., Graham, M. E., Gabrielli, B. G., Robinson, P. J., Nigg, E. A., Ono, Y. et al. (2005). Cdk1/Erk2- and Plk1-dependent phosphorylation of a centrosome protein, Cep55, is required for its recruitment to midbody and cytokinesis. *Dev. Cell* **9**, 477-488. doi:10.1016/j.devcel.2005.09.003
Foley, E. A. and Kapoor, T. M. (2013). Microtubule attachment and spindle assembly checkpoint signalling at the kinetochore. *Nat. Rev. Mol. Cell Biol.* **14**, 25-37. doi:10.1038/nrm3494
Forester, C. M., Maddox, J., Louis, J. V., Goris, J. and Virshup, D. M. (2007). Control of mitotic exit by PP2A regulation of Cdc25C and Cdk1. *Proc. Natl. Acad. Sci. USA* **104**, 19867-19872. doi:10.1073/pnas.0709879104
Gershony, O., Pe'er, T., Noach-Hirsh, M., Elia, N. and Tzur, A. (2014). Cytokinetic abscission is an acute G1 event. *Cell Cycle* **13**, 3436-3441. doi:10.4161/15384101.2014.956486
Greaney, J., Wei, Z. and Homer, H. (2018). Regulation of chromosome segregation in oocytes and the cellular basis for female meiotic errors. *Hum. Reprod. Update* **24**, 135-161. doi:10.1093/humupd/dmx035
Gui, L. and Homer, H. (2012). Spindle assembly checkpoint signalling is uncoupled from chromosomal position in mouse oocytes. *Development* **139**, 1941-1946. doi:10.1242/dev.078352
Gui, L. and Homer, H. (2013). Hec1-dependent cyclin B2 stabilization regulates the G2-M transition and early prometaphase in mouse oocytes. *Dev. Cell* **25**, 43-54. doi:10.1016/j.devcel.2013.02.008
Hached, K., Xie, S. Z., Buffin, E., Cladifre, D., Rachez, C., Sacras, M., Sorger, P. K. and Wassmann, K. (2011). Mps1 at kinetochores is essential for female mouse meiosis I. *Development* **138**, 2261-2271. doi:10.1242/dev.061317
Han, S. J., Chen, R., Paronetto, M. P. and Conti, M. (2005). Wee1B is an oocyte-specific kinase involved in the control of meiotic arrest in the mouse. *Curr. Biol.* **15**, 1670-1676. doi:10.1016/j.cub.2005.07.056
Hauf, S., Waizenegger, I. C. and Peters, J. M. (2001). Cohesin cleavage by separase required for anaphase and cytokinesis in human cells. *Science* **293**, 1320-1323. doi:10.1126/science.1061376
Herbert, M., Levasseur, M., Homer, H., Yallop, K., Murdoch, A. and Mcdougall, A. (2003). Homologue disjunction in mouse oocytes requires proteolysis of securin and cyclin B1. *Nat. Cell Biol.* **5**, 1023-1025. doi:10.1038/ncb1062
Homer, H. A. (2013). The APC/C in female mammalian meiosis I. *Reproduction* **146**, R61-R71. doi:10.1530/REP-13-0163
Homer, H. A., Gui, L. and Carroll, J. (2009). A spindle assembly checkpoint protein functions in prophase I arrest and prometaphase progression. *Science* **326**, 991-994. doi:10.1126/science.1175326
Homer, H. A., Mcdougall, A., Levasseur, M., Murdoch, A. P. and Herbert, M. (2005a). Mad2 is required for inhibiting securin and cyclin B degradation following spindle depolymerisation in meiosis I mouse oocytes. *Reproduction* **130**, 829-843. doi:10.1530/rep.1.00856
Homer, H. A., Mcdougall, A., Levasseur, M., Yallop, K., Murdoch, A. and Herbert, M. (2005b). Mad2 prevents aneuploidy and premature proteolysis of cyclin B and securin during meiosis I in mouse oocytes. *Genes Dev.* **19**, 202-207. doi:10.1101/gad.328105
Jones, K. T. and Lane, S. I. (2013). Molecular causes of aneuploidy in mammalian eggs. *Development* **140**, 3719-3730. doi:10.1242/dev.090589
Kalimutho, M., Sinha, D., Jeffery, J., Nones, K., Srihari, S., Fernando, W. C., Duijf, P. H., Vennin, C., Raninga, P., Nanayakkara, D. et al. (2018). CEP55 is a determinant of cell fate during perturbed mitosis in breast cancer. *EMBO Mol. Med.* **10**, e8566. doi:10.15252/emmm.201708566
Kolano, A., Brunet, S., Silk, A. D., Cleveland, D. W. and Verlhac, M.-H. (2012). Error-prone mammalian female meiosis from silencing the spindle assembly checkpoint without normal interkinetochore tension. *Proc. Natl. Acad. Sci. USA* **109**, E1858-E1867. doi:10.1073/pnas.1204686109
Kudo, N. R., Wassmann, K., Anger, M., Schuh, M., Wirth, K., Xu, H., Helmhart, W., Kudo, H., Mckay, M., Maro, B. et al. (2006). Resolution of chiasmata in oocytes requires separase-mediated proteolysis. *Cell* **126**, 135-146. doi:10.1016/j.cell.2006.05.033
Lane, S. I. R. and Jones, K. T. (2014). Non-canonical function of spindle assembly checkpoint proteins after APC activation reduces aneuploidy in mouse oocytes. *Nat. Commun.* **5**, 3444. doi:10.1038/ncomms4444
Lane, S. I. R., Yun, Y. and Jones, K. T. (2012). Timing of anaphase-promoting complex activation in mouse oocytes is predicted by microtubule-kinetochore attachment but not by bivalent alignment or tension. *Development* **139**, 1947-1955. doi:10.1242/dev.077040
Levasseur, M., Thomas, C., Davies, O. R., Higgins, J. M. G. and Madgwick, S. (2019). Aneuploidy in oocytes is prevented by sustained CDK1 activity through degron masking in cyclin B1. *Dev. Cell* **48**, 672-684. doi:10.1016/j.devcel.2019.01.008
Lincoln, A. J., Wickramasinghe, D., Stein, P., Schultz, R. M., Palko, M. E., De Miguel, M. P. D., Tessarollo, L. and Donovan, P. J. (2002). Cdc25b phosphatase is required for resumption of meiosis during oocyte maturation. *Nat. Genet.* **30**, 446-449. doi:10.1038/ng856
Lukinavičius, G., Reymond, L., D'este, E., Masharina, A., Göttfert, F., Ta, H., Güther, A., Fournier, M., Rizzo, S., Waldmann, H. et al. (2014). Fluorogenic probes for live-cell imaging of the cytoskeleton. *Nat. Methods* **11**, 731-733. doi:10.1038/nmeth.2972
Malumbres, M. (2014). Cyclin-dependent kinases. *Genome Biol.* **15**, 122. doi:10.1186/gb4184
Martinez-Garay, I., Rustom, A., Gerdes, H.-H. and Kutsche, K. (2006). The novel centrosomal associated protein CEP55 is present in the spindle midzone and the midbody. *Genomics* **87**, 243-253. doi:10.1016/j.ygeno.2005.11.006
Meadows, J. C. and Millar, J. B. A. (2015). Sharpening the anaphase switch. *Biochem. Soc. Trans.* **43**, 19-22. doi:10.1042/BST20140250
Morita, E., Sandrin, V., Chung, H.-Y., Morham, S. G., Gygi, S. P., Rodesch, C. K. and Sundquist, W. I. (2007). Human ESCRT and ALIX proteins interact with proteins of the midbody and function in cytokinesis. *EMBO J.* **26**, 4215-4227. doi:10.1038/sj.emboj.7601850
Oh, J. S., Han, S. J. and Conti, M. (2010). Wee1B, Myt1, and Cdc25 function in distinct compartments of the mouse oocyte to control meiotic resumption. *J. Cell Biol.* **188**, 199-207. doi:10.1083/jcb.200907161
Oh, J. S., Susor, A. and Conti, M. (2011). Protein tyrosine kinase Wee1B is essential for metaphase II exit in mouse oocytes. *Science* **332**, 462-465. doi:10.1126/science.1199211
Pesin, J. A. and Orr-Weaver, T.-L. (2008). Regulation of APC/C activators in mitosis and meiosis. *Annu. Rev. Cell Dev. Biol.* **24**, 475-499. doi:10.1146/annurev.cellbio.041408.115949
Sackton, K. L., Dimova, N., Zeng, X., Tian, W., Zhang, M., Sackton, T. B., Meaders, J., Pfaff, K. L., Sigoillot, F., Yu, H. et al. (2014). Synergistic blockade of mitotic exit by two chemical inhibitors of the APC/C. *Nature* **514**, 646-649. doi:10.1038/nature13660
Sebestova, J., Danylevska, A., Novakova, L., Kubelka, M. and Anger, M. (2012). Lack of response to unaligned chromosomes in mammalian female gametes. *Cell Cycle* **11**, 3011-3018. doi:10.4161/cc.21398
Stemmann, O., Zou, H., Gerber, S. A., Gygi, S. P. and Kirschner, M. W. (2001). Dual inhibition of sister chromatid separation at metaphase. *Cell* **107**, 715-726. doi:10.1016/S0092-8674(01)00603-1
Strauss, B., Harrison, A., Coelho, P. A., Yata, K., Zernicka-Goetz, M. and Pines, J. (2018). Cyclin B1 is essential for mitosis in mouse embryos, and its nuclear export sets the time for mitosis. *J. Cell Biol.* **217**, 179-193. doi:10.1083/jcb.201612147
Sullivan, M. and Morgan, D. O. (2007). Finishing mitosis, one step at a time. *Nat. Rev. Mol. Cell Biol.* **8**, 894-903. doi:10.1038/nrm2276
Terret, M., Wassmann, K., Waizenegger, I., Maro, B., Peters, J.-M. and Verlhac, M.-H. (2003). The meiosis I-to-meiosis II transition in mouse oocytes requires separase activity. *Curr. Biol.* **13**, 1797-1802. doi:10.1016/j.cub.2003.09.032
Thomas, Y., Coux, O. and Baldin, V. (2010). betaTrCP-dependent degradation of CDC25B phosphatase at the metaphase-anaphase transition is a pre-requisite for correct mitotic exit. *Cell Cycle* **9**, 4338-4350. doi:10.4161/cc.9.21.13593
Van Der Horst, A., Simmons, J. and Khanna, K. K. (2009). Cep55 stabilization is required for normal execution of cytokinesis. *Cell Cycle* **8**, 3742-3749. doi:10.4161/cc.8.22.10047
Waizenegger, I., Giménez-Abian, J. F., Wernic, D. and Peters, J.-M. (2002). Regulation of human separase by securin binding and autocleavage. *Curr. Biol.* **12**, 1368-1378. doi:10.1016/S0960-9822(02)01073-4
Wassmann, K., Niault, T. and Maro, B. (2003). Metaphase I arrest upon activation of the MAD2-dependent spindle checkpoint in mouse oocytes. *Curr. Biol.* **13**, 1596-1608. doi:10.1016/j.cub.2003.08.052
Waters, J. C., Chen, R.-H., Murray, A. W. and Salmon, E. D. (1998). Localization of Mad2 to kinetochores depends on microtubule attachment, not tension. *J. Cell Biol.* **141**, 1181-1191. doi:10.1083/jcb.141.5.1181
Wei, Z., Greaney, J., Zhou, C. and Homer, A. H. (2018). Cdk1 inactivation induces post-anaphase-onset spindle migration and membrane protrusion required for

extreme asymmetry in mouse oocytes. *Nat. Commun.* **9**, 4029. doi:10.1038/s41467-018-06510-9

Wolf, F., Sigl, R. and Geley, S. (2007). 'The end of the beginning': cdk1 thresholds and exit from mitosis. *Cell Cycle* **6**, 1408-1411. doi:10.4161/cc.6.12.4361

Wolf, F., Wandke, C., Isenberg, N. and Geley, S. (2006). Dose-dependent effects of stable cyclin B1 on progression through mitosis in human cells. *EMBO J.* **25**, 2802-2813. doi:10.1038/sj.emboj.7601163

Xu, Z.-Y., Ma, X.-S., Qi, S.-T., Wang, Z.-B., Guo, L., Schatten, H., Sun, Q.-Y. and Sun, Y.-P. (2015). Cep55 regulates spindle organization and cell cycle progression in meiotic oocyte. *Sci. Rep.* **5**, 16978. doi:10.1038/srep16978

Zhao, W.-M., Seki, A. and Fang, G. (2006). Cep55, a microtubule-bundling protein, associates with centralspindlin to control the midbody integrity and cell abscission during cytokinesis. *Mol. Biol. Cell* **17**, 3881-3896. doi:10.1091/mbc.e06-01-0015

Supplementary Information

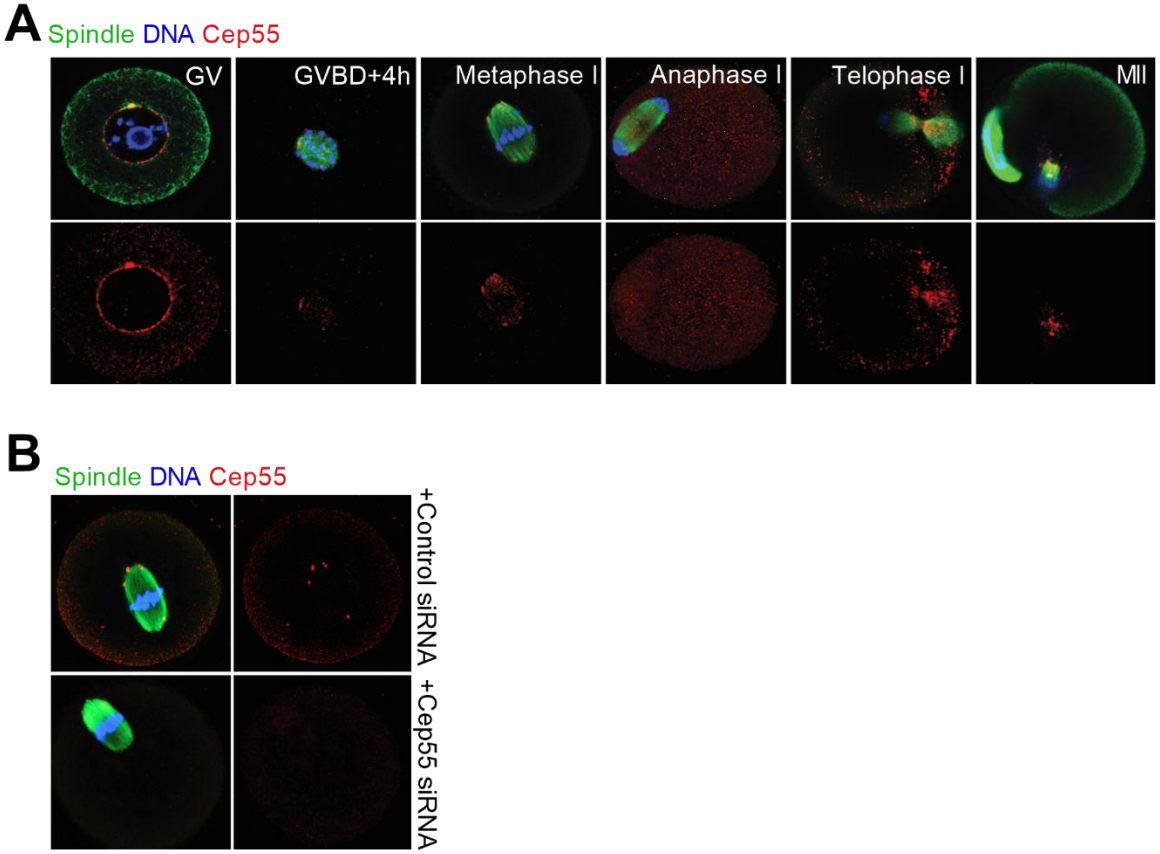

Fig. S1. Cep55 localisation during MI and following Cep55 siRNA microinjection. (A) Localization of endogenous Cep55 in mouse oocytes during meiotic maturation. Shown are representative images of oocytes at the stages shown immunostained for Cep55, spindle microtubules and chromosomes. (B) Cep55 spindle pole labelling is lost in oocytes injected with Cep55 siRNA whilst spindle assembly and chromosome alignment remain intact. Shown are representative images of mock-depleted (n = 45) and Cep55-depleted (n = 23) oocytes immunostained for Cep55, spindle microtubules and chromosomes. Note that following assembly of the bipolar spindle, Cep55 localises as discrete foci in the region of spindle poles in mock-depleted oocytes. Note also that spindle assembly and chromosome alignment remain intact whilst spindle pole labelling is lost in oocytes injected with Cep55 siRNA. Results are representative of at least three independent experiments.

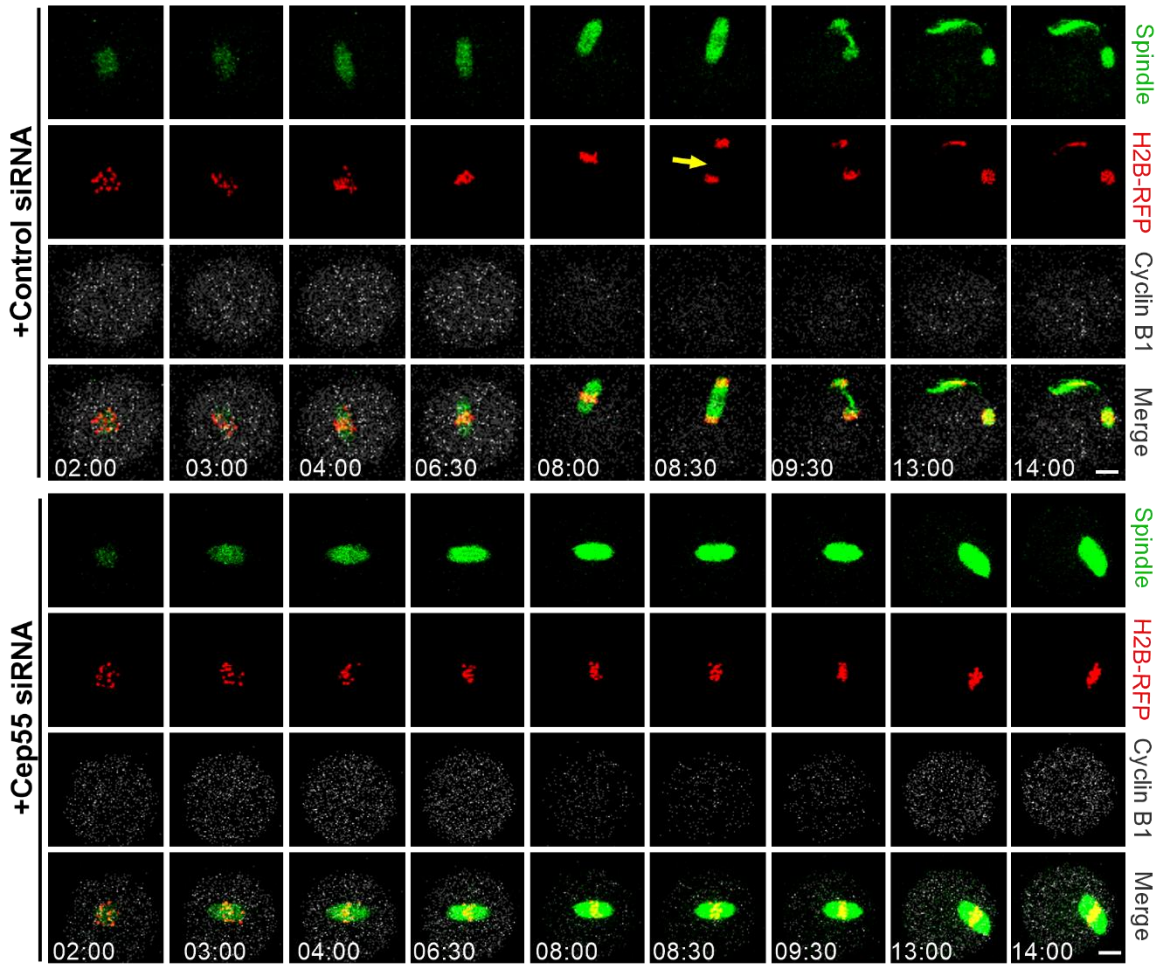

Fig. S2. Cep55-depletion induces anaphase-failure without preventing cyclin B1 proteolysis. Shown are images from representative timelapse series of mock-depleted (*n* = 12) and Cep55-depleted (*n* =15) oocytes expressing H2B-RFP and cyclin B1-GFP and stained with SiR-tubulin for labelling spindles. Note that in both groups of oocytes, cyclin B1-GFP fluorescence declines to a nadir around 8-8.5 h post-GVBD (reflecting proteolysis) and partially recovers around 13 h post-GVBD but anaphase only occurs in mock-depleted oocytes. Yellow arrow, anaphase I. Time is hh:mm post-GVBD. Scale bars, 10 µm. Results are representative of at least three independent experiments.

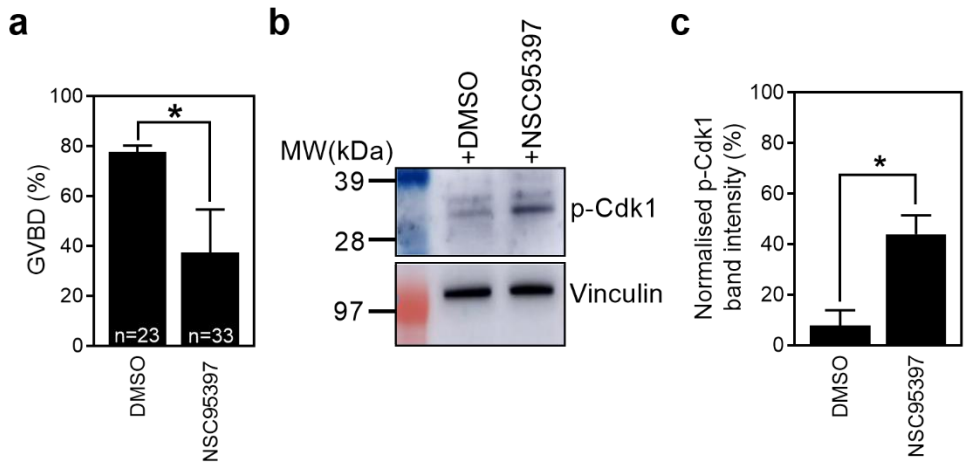

Fig. S3. The Cdc25B inhibitor, NSC95397, inhibits Cdk1 activity in mouse oocytes by promoting inhibitory Cdk1 phosphorylation. (A) GVBD is significantly inhibited in GV-stage oocytes treated with NSC95397. Note that GVBD is reduced by half following treatment with NSC95397. (B and C). NSC95397 significantly increases p-Cdk1 levels in GV-stage oocytes. Shown is a representative Western blot of p-Cdk1. Vinculin served as a loading control. $n = 50$ oocytes per lane (B). Graph shows the average p-Cdk1 band intensity from three experiments (C). Data are mean ± s.e.m. $*p < 0.05$ (Student's t test). Results are representative of at least three independent experiments.

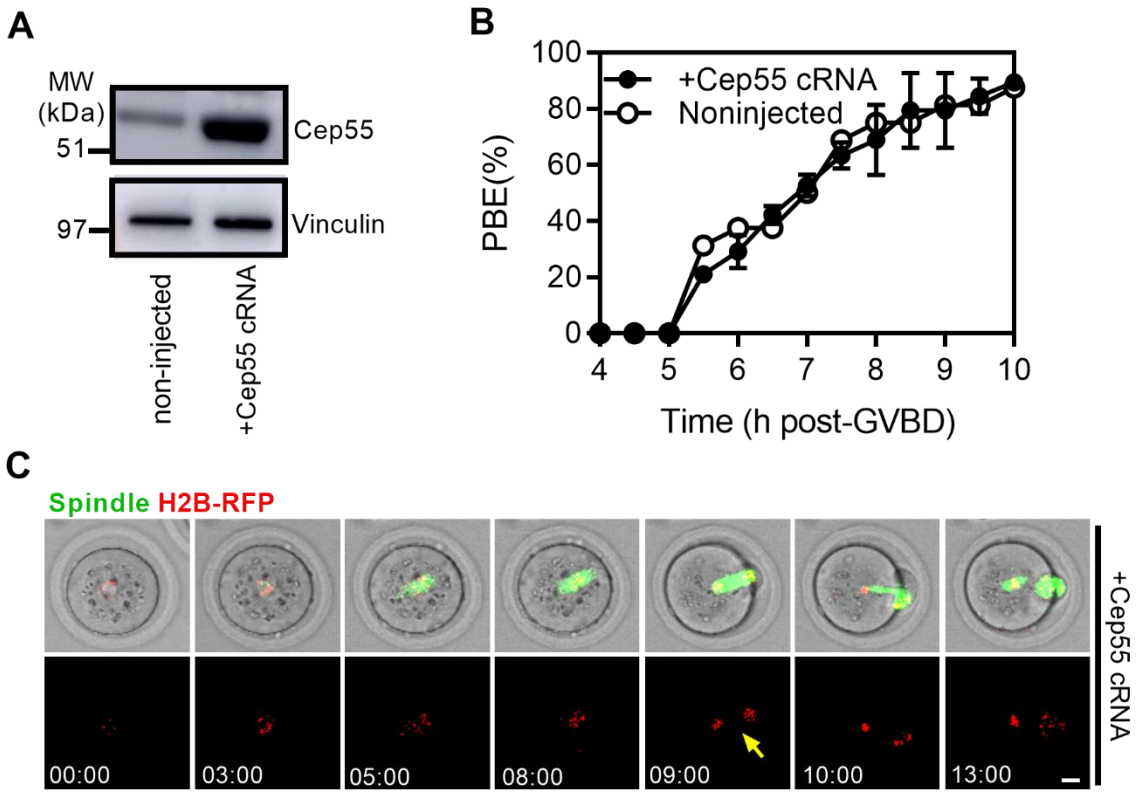

Fig. S4. Cep55 overexpression has no effect on the timing of anaphase I or PBE. (A) Shown is a representative Western blot of oocytes that were microinjected with Cep55 cRNA. Vinculin served as a loading control. *n* = 30 oocytes per lane. (B) Rates of polar body extrusion (PBE) in non-injected and Cep55 cRNA injected oocytes. (C) Representative timelapse images of spindles and chromosomes during meiotic maturation in live oocytes over-expressing Cep55 (*n* = 25 oocytes). Yellow arrow, anaphase. Time is hh:mm post-GVBD. Scale bar, 10 µm.

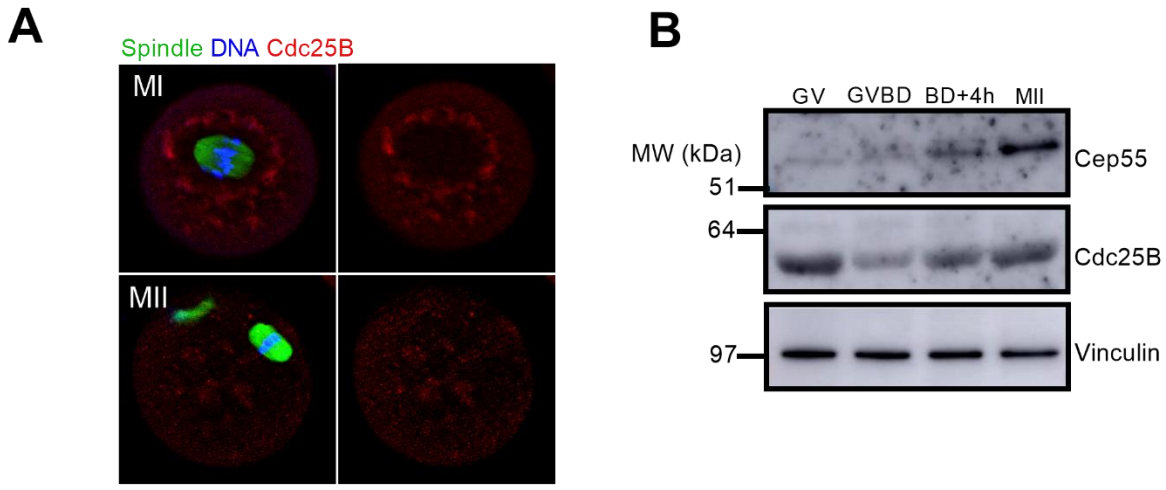

Fig. S5. Cdc25B localisation and expressing level during MI and MII. (A) Shown are representative images of oocytes at the stages shown immunostained for Cdc25B, spindle microtubules and chromosomes (n = 12 oocytes). Note the diffuse cytoplasmic localisation. (B) Endogenous levels of Cep55 and Cdc25B throughout meiotic maturation in mouse oocytes. Shown is a representative Western blot of Cep55 and Cdc25b. Vinculin served as a loading control. n = 30 oocytes per lane.

Movies

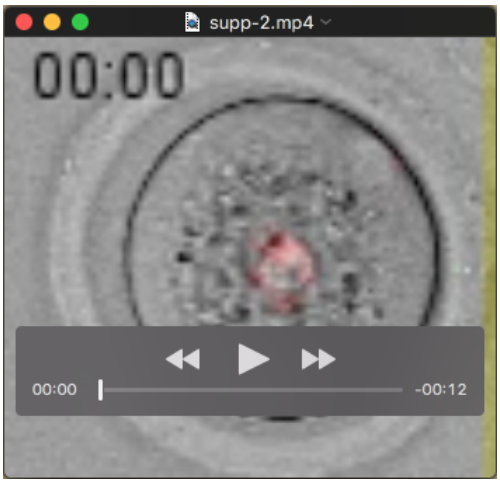

Movie 1. Spindle assembly, chromosome alignment, anaphase I and PBE in a control oocyte. Timelapse imaging of an oocyte expressing H2B-RFP (red) and stained with SiR-tubulin dye (green). Time scale is shown in hh:mm. Note that a bipolar spindle assembles slowly close to the centre of the oocyte prior to migrating to the oocyte cortex and undergoing anaphase I around 9 h post-GVBD followed accompanied very shortly after by PBE.

Movie 2. Spindle assembly and chromosome alignment without anaphase I in a Cep55-depleted oocyte. Timelapse imaging of a Cep55-depleted oocyte expressing H2B-RFP (red) and stained with SiR-tubulin dye (green). Time scale is shown in hh:mm. Note that a bipolar spindle assembles and chromosomes align normally but that anaphase I fails to occur even by 19 h post-GVBD.

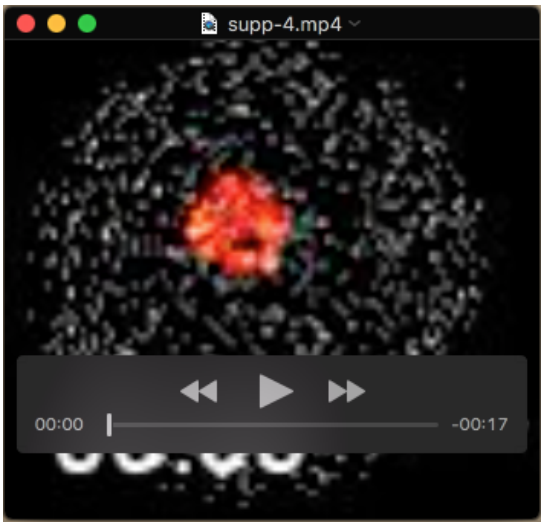

Movie 3. Spindle assembly, chromosome alignment, securin proteolysis, anaphase I and PBE in a mock-depleted oocyte. Timelapse imaging of an oocyte expressing H2B-RFP (red) and securin-GFP (monochrome) and stained with SiR-tubulin dye (green). Time scale is shown in hh:mm. Note that a bipolar spindle assembles, chromosomes align and anaphase I occurs around 8 h post-GVBD concurrently with which, securin-GFP levels reach a nadir followed very shortly after by PBE, entry into MII and partial recovery of securin-GFP levels.

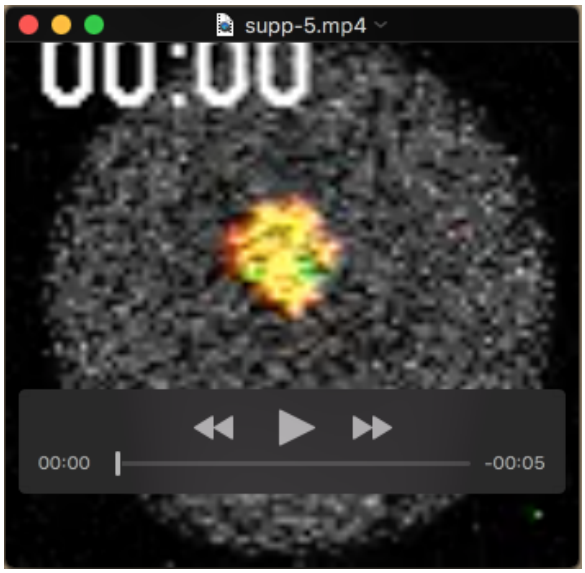

Movie 4. Spindle assembly, chromosome alignment and securin proteolysis without anaphase I or PBE in a Cep55-depleted oocyte. Timelapse imaging of an oocyte expressing H2B-RFP (red) and securin-GFP (monochrome) and stained with SiR-tubulin dye (green). Time scale is shown in hh:mm. Note that a bipolar spindle assembles, chromosomes align and securin-GFP reaches a nadir around 8-8.5 h post-GVBD followed by recovery but that neither anaphase I nor PBE occur.

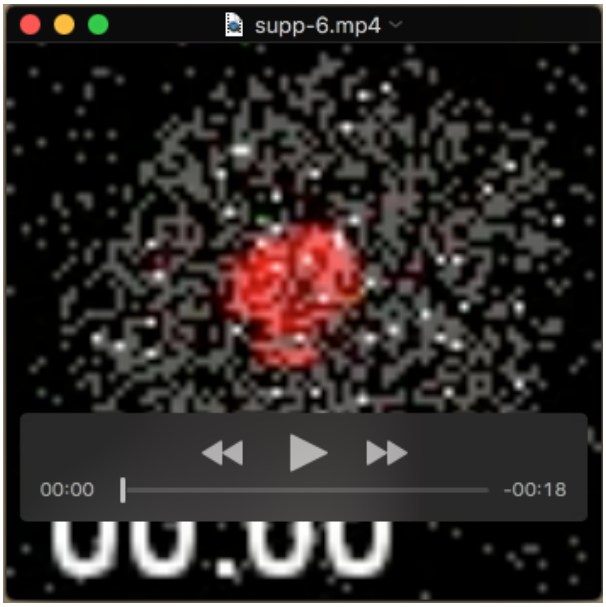

Movie 5. Spindle assembly, chromosome alignment, cyclin B1 proteolysis, anaphase I and PBE in a mock-depleted oocyte. Timelapse imaging of an oocyte expressing H2B-RFP (red) and cyclin B1-GFP (monochrome) and stained with SiR-tubulin dye (green). Time scale is shown in hh:mm. Note that a bipolar spindle assembles, chromosomes align and anaphase I occurs around 9 h post-GVBD concurrently with which, cyclin B1-GFP levels reach a nadir followed very shortly after by PBE, entry into MII and partial recovery of cyclin B1-GFP levels.

Movie 6. Spindle assembly, chromosome alignment and cyclin B1 proteolysis without anaphase I or PBE in a Cep55-depleted oocyte. Timelapse imaging of an oocyte expressing H2B-RFP (red) and cyclin B1-GFP (monochrome) and stained with SiR-tubulin dye (green). Time scale is shown in hh:mm. Note that a bipolar spindle assembles, chromosomes align and securin-GFP reaches a nadir around 8.5 h post-GVBD followed by partial recovery but that neither anaphase I nor PBE occur.

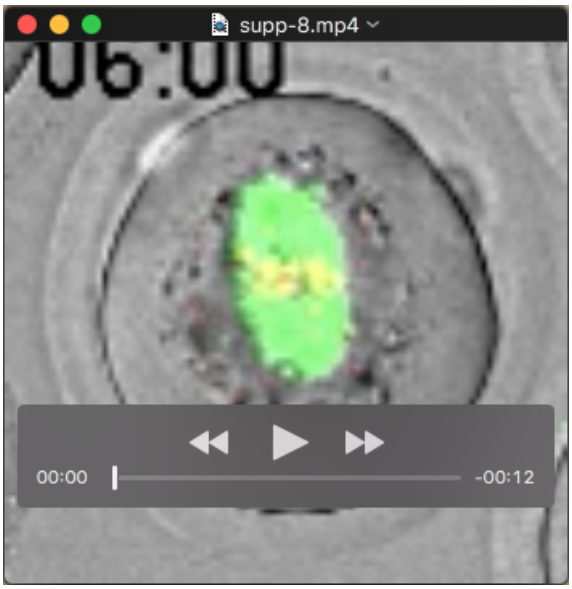

Movie 7. Forced Cdk1 inactivation by flavopiridol induces anaphase I and PBE in Cep55-depleted oocytes. Timelapse imaging of a Cep55-depleted oocyte expressing H2B-RFP (red) and stained with SiR-tubulin dye (green) treated with flavopiridol from 6 h post-GVBD. Time scale is shown in hh:mm. Note that anaphase I occurs by 30 min following treatment and is followed by PBE that is apparent by 1.5 hours. Note also that chromosomes eventually decondense due to persistent Cdk1 inactivation induced by flavopiridol.

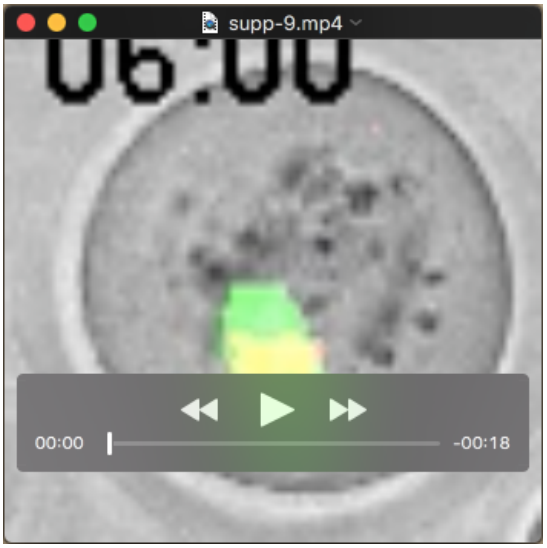

Movie 8. Treatment with DMSO solvent does not induce anaphase I or PBE in Cep55-depleted oocytes. Timelapse imaging of a Cep55-depleted oocyte expressing H2B-RFP (red) and stained with SiR-tubulin dye (green) treated with DMSO solvent from 6 h post-GVBD. Time scale is shown in hh:mm. Note that neither anaphase nor PBE occur.

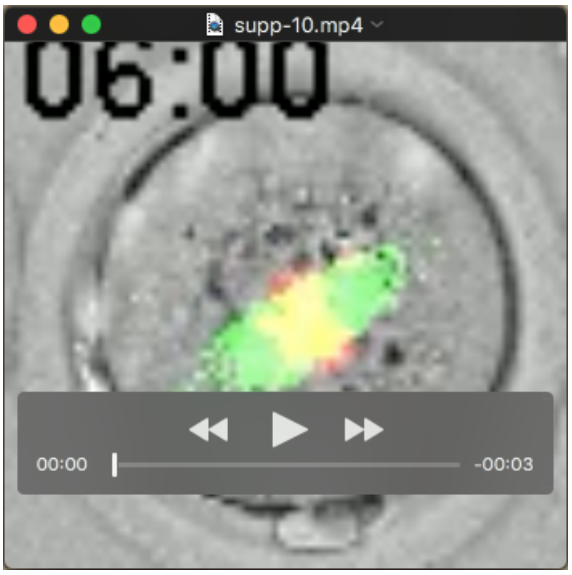

Movie 9. DMSO does not prevent anaphase I and PBE in control oocytes. Timelapse imaging of a control oocyte expressing H2B-RFP (red) and stained with SiR-tubulin dye (green) treated with DMSO solvent from 6 h post-GVBD. Time scale is shown in hh:mm.

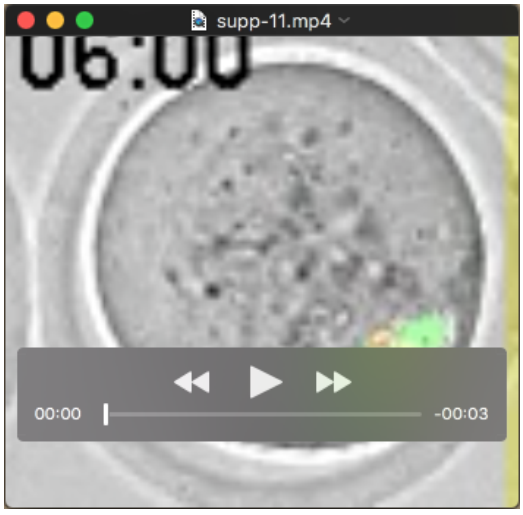

Movie 10. The Wee1 inhibitor, MK1775, prevents anaphase I and PBE in control oocytes. Timelapse imaging of a control oocyte expressing H2B-RFP (red) and stained with SiR-tubulin dye (green) treated with MK1775 from 6 h post-GVBD. Time scale is shown in hh:mm. Note that anaphase I and PBE do not occur even by 15 h post-GVBD.

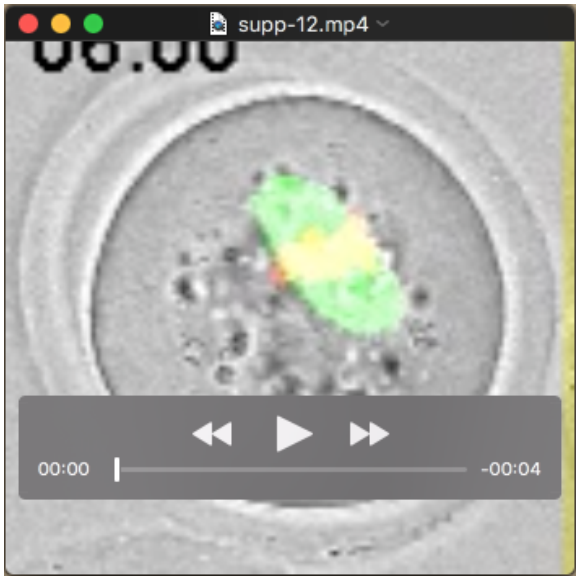

Movie 11. DMSO does not induce anaphase I and PBE in Cep55-depleted oocytes. Timelapse imaging of a Cep55-depleted oocyte expressing H2B-RFP (red) and stained with SiR-tubulin dye (green) treated with DMSO solvent from 6 h post-GVBD. Time scale is shown in hh:mm. Note that anaphase I and PBE do not occur even by 18 h post-GVBD.

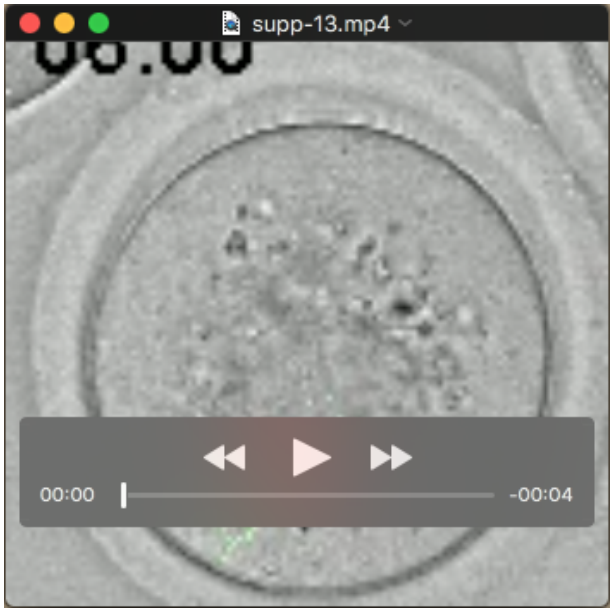

Movie 12. The Cdc25B inhibitor, NSC95397, induces anaphase and PBE in Cep55-depleted oocytes. Timelapse imaging of a Cep55-depleted oocyte expressing H2B-RFP (red) and stained with SiR-tubulin dye (green) treated with NSC95397 from 6 h post-GVBD. Time scale is shown in hh:mm. Note that anaphase I and PBE occur by 10 h post-GVBD.